Bilateral visual projections exist in non-teleost bony fish and predate the emergence of tetrapods

Robin J Vigouroux, Karine Duroure, Juliette Vougny, Shahad Albadri, Peter Kozulin, Eloisa Herrera, Kim Nguyen-Ba-Charvet, Ingo Braasch, Rodrigo Suárez, Filippo del Bene, et al.

Bilateral visual projections exist in non-teleost bony fish and predate the emergence of tetrapods

One sentence summary: Bilateral vision preceded terrestrial life

Robin J. Vigouroux[1], Karine Duroure[1], Juliette Vougny[2], Shahad Albadri[1], Peter Kozulin[3], Eloisa Herrera[4], Kim Nguyen-Ba-Charvet[1], Ingo Braasch[5], Rodrigo Suárez[3], Filippo Del Bene[1]* and Alain Chédotal[1]*

*Corresponding authors.

Email: filippo.delbene@inserm.fr and Email: alain.chedotal@inserm.fr

[1]Sorbonne Université, INSERM, CNRS, Institut de la Vision, 17 Rue Moreau, 75012 Paris, France

[2]Institut Curie, PSL Research University, INSERM U934, CNRS UMR3215, Paris, France

[3]Queensland Brain Institute, The University of Queensland, Building 79, St Lucia Campus, Brisbane, QLD 4072, Australia

[4]Instituto de Neurociencias Av. Ramón y Cajal s/n San Juan de Alicante 03550 Spain

[5]Department of Integrative Biology and Program in Ecology, Evolution and Behavior, Michigan State University, 288 Farm Lane, East Lansing MI 48824, USA

Abstract:

In most vertebrates, camera-style eyes contain retinal ganglion cell neurons projecting to visual centers on both sides of the brain. However, in fish, ganglion cells are thought to only innervate the contralateral side. This suggested that bilateral visual projections appeared in tetrapods. Here, we show that bilateral visual projections exist in non-teleost fishes and that the appearance of ipsilateral projections does not correlate with terrestrial transition or predatory behavior. We also report that the developmental program specifying visual system laterality differs between fishes and mammals as the Zic2 transcription factor which specifies ipsilateral retinal ganglion cells in tetrapods appears absent from fish ganglion cells. However, overexpressing human ZIC2 induces ipsilateral visual projections in zebrafish. Therefore, the existence of bilateral visual projections likely preceded the emergence of binocular vision in tetrapods.

Eye position on the head is highly variable between species, but frontal eyes have long been considered critical for depth perception (stereopsis) by increasing the overlap of the right and left eye visual fields (*1*). In vertebrates, ganglion cell axons from each eye cross through each other at the optic chiasm and enter the brain on the contralateral side. In mammals, visual axons from each eye meet and interweave at the chiasm. However, optic nerve crossing modalities are more diverse in fish and in most species the two optic nerves remain fully separated and only overlap at the chiasm (*2*, *3*).

Classic neuroanatomical studies showed that in mammals, eye projections are bilateral with a variable fraction of retinal ganglion cell (referred to as ganglion cell thereafter) axons continuing in the ipsilateral optic tract after crossing the chiasm. The proportion of ipsilateral projections is low (2-3%) in rodents but reaches around 40% in primates (*4*, *5*). The comparative analysis of many vertebrate species conducted over several decades suggests that ipsilateral visual axons exist in all mammals, anuran amphibians, some reptiles, and that they are essentially absent or were secondarily lost in birds (*5*–*8*). Accordingly, developmental transcriptional programs specifying ipsilateral ganglion cells described in mammals are conserved in Xenopus but not in chick and zebrafish (*5*, *9*). This textbook view implies that visual axon bilaterality emerged in early tetrapods and might have provided a visual advantage, in particular for nocturnal and predatory terrestrial species (*10*). However, a review of the extensive literature on fish visual systems gives a more complex image with reports, sometimes contradictory, of ipsilateral ganglion cell projections in some fish species (*6*, *11*). Most of these pioneering studies relied on imprecise histological staining methods such as the Nauta-Gygax staining method or autoradiography (*12*). Here, we assessed the laterality of visual projections in bony fishes (**Fig. 1A**) with the B fragment of the cholera toxin (*12*) coupled to fluorescent dyes. Dye-coupled Cholera toxins have not been previously used in fish although they proved to be highly reliable tracers for visual projections in rodents due to their efficient endocytosis by neurons, slow elimination, high photostability and brightness (*13*). They are also compatible with whole-brain clearing and thereby allow mapping visual pathways in intact brain using 3D light sheet fluorescence microscopy (*14*, *15*).

With more than 30,000 species, fishes account for at least half of the extant vertebrate species (*16*). We initially focused on ray-finned fishes (Actinopterygians; **Fig. 1A** and **fig. S1**) which separated from lobe-finned fish (Sarcopterygians, including tetrapods) around 450 Million years ago (Ma)(*17*). Within ray-finned fishes, we initially selected 6 species among the clupeocephalan lineage (**fig. S1**), the largest of the three lineages of teleost fishes which account for most (about 96%) of extant teleosts (*18*). Within clupeocephalans, three represent ostariophysians (Mexican tetra *Astyanax mexicanus*, redeye piranha *Serrasalmus rhombeus*, and zebrafish *Danio rerio*) and three are percomorphs (green-spotted pufferfish *Tetraodon nigroviridis*, Atlantic mudskipper *Periophtalmus barbarus,* and four-eyed fish *Anableps anableps*). With 9,000 and 16,000 species respectively, ostariophysians and percomorphs are the two largest clades of teleosts. They have diverse eye positions, feeding behaviors, and habitats and some were previously reported to have ipsilateral visual projections (*11*).

Totally crossed visual projections in teleosts

The visual system of the zebrafish has been extensively studied using lipophilic dye tracing or genetic methods and shown to be exclusively contralateral (*19*). Accordingly, we found that fluorescent (Cholera toxin labelled) axons were only present on the contralateral side of adult zebrafish brains (**Fig. 1B** and **movie S1**; n=6). Previously identified retino-recipient visual nuclei (*20*) could be detected with cholera toxin, thereby validating the use of this tracing method in fish (**Fig. 1C**). Light-sheet microscopy imaging of cholera toxin injected fish, showed that visual projections were only contralateral in Mexican tetra surface fish (**Fig. 1, D** and **E** and **movie S1;** n=7), contradicting a previous study (*21*). Likewise, eyes in the redeye piranha only projected contralaterally (**Fig. 1, F** and **G** and **movie S1**; n= 3), in disagreement with earlier work in other piranha species (*22*, *23*). This suggests that ostariophysians only have crossed visual projections.

In the fresh water green-spotted pufferfish (*24*), a percomorph, the 2 optic nerves stay separated at the chiasm and visual projections were exclusively contralateral (**Fig. 1, H** and **I** and **fig. S2** and **movie S1**; n= 4) as previously described in another pufferfish (*25*). We next studied the four-eyed fish, a percomorph surface dweller fish whose large protruding eyes with duplicated corneas and pupils allows seeing under and above the water (*26*). Again, one optic nerve passed over the other at the chiasm (**fig. S2**) and cholera toxin tracing showed that in this species, visual projections were also completely crossed (**Fig. 1, J** and **K**; n= 3). Similar results were obtained in the mudskipper, a percomorph with amphibious lifestyle (**Fig. 1, L** and **M** and **fig. S2** and **movie S1**; n= 3). Together, these results show that in percomorph eyes, ganglion cells also likely only project to visual nuclei on the opposite side of the brain (**fig. S1**).

Osteoglossomorphs (bonytongues), a teleost sister groups of clupeocephalans (**Fig. 1A** and **fig. S1**), are considered a group of basal (i.e the group which gave rise to later forms) teleosts constituted of about 200 living species (*16*). We chose to trace visual projections in the African butterflyfish (*Pantodon buchholzi*), a predator living close to the surface of freshwater system, and found a small contingent of retinal axons (**Fig. 2, A** and **B** and **movie S1,** 2.33±0.23 % ipsilateral projections in the optic tectum; n=3) project to the ipsilateral side, corroborating an earlier report (*27*). The main portion of ipsilateral axons targeted the tectum and some others targeted pretectal nuclei. Ipsilateral visual axons have also been described in a mormyrid electric fish (*Gnathonemus petersii*) (*28*), another osteoglossomorph with a more nocturnal predatory behavior that can orient by active electrolocation (*29*). These results show that bilateral visual projections exist in osteoglossomorph teleosts regardless of their predatory strategy and lifestyle history. Therefore, within teleosts, ipsilateral projections could have been secondarily lost in clupeocephalans or independently acquired in osteoglossomorphs. In mammals, binocular inputs to visual targets/areas are either segregated (thalamus, colliculus) or intermingled (suprachiasmatic nucleus). As both eyes were injected with 2 distinct Alexa-conjugated-cholera toxins, we also studied the relative distribution of ipsilateral and contralateral ganglion cell axons in butterflyfish brain areas innervated by both eyes. This showed that in African butterflyfish (**Fig. 2C**) retinal inputs from both sides segregated, as in the thalamus and superior colliculus of mammals.

Bilateral visual projections exist in basal ray-finned fishes

These results on teleosts led us to study retinal projections in non-teleost ray-finned fish lineages (Holosteans, Acipenseriforms, and Polypteriforms, **Fig. 1A**) which split from teleosts before the teleost whole genome duplication event (TGD, **Fig. 1A**) that occurred around 320 Ma in the ancestor of extant teleosts (reviewed in (*30*)). Holosteans and Acipenseriforms are considered to have evolved slowly since they branched from other vertebrates 350 Ma (*31*). Bilateral visual projections (**movie S2**, n=5/5) were observed in the spotted gar (*Lepisosteus oculatus*), one of the seven extant species of garfish, and a representative of the holosteans. The spotted gar is a unique vertebrate model system as its genome is thought to provide a "bridge" between tetrapods and teleosts (*32*). Bilateral cholera toxin injections revealed an ipsilateral projection in the rostral optic tectum of the spotted gar, with visual axons targeting several pretectal nuclei. There was no overlap of the contralateral and ipsilateral axons (**Fig. 2, D** to **F** and **movie S2**, n=5/5) which represented 4.78±0.46 % of visual inputs in the tectum, a ratio comparable to rodents. Next, we traced visual projections in the acipenseriform sterlet sturgeon (*Acipenser ruthenus*, n=2/2). Cholera toxin tracing demonstrated the existence of a binocular domain in the tectum of the sterlet sturgeon as well as in several pretectal nuclei (**Fig. 2, G** to **J** and **movie S2**; 9.77±1.28 % ipsilateral projections in the tectum, n=2). No re-crossing of visual inputs after entering the brain were detected contrary to previous observations in the Russian sturgeon *Acipenser güldenstädtii* (*33*). We then studied the armored bichir (*Polypterus delhezi*; n=2/2), a carnivorous nocturnal fish representing the most basally diverging lineage of extant ray-finned fishes, the Polypteriforms. In the bichir, the two optic nerves meet at the chiasm and ganglion cells axons interweave during decussation (**fig. S2**). Ipsilateral axons projected to numerous pretectal nuclei such as the nucleus opticus dorsolateralis anterior thalami, the area optica ventrolateralis thalami, and the nucleus commissurae posterior par magnocellularis (**Fig. 2, K** to **N** and **movie S2**). This corroborates previous studies in gray bichir *Polypterus senegalus* (*34*). These results, together with similar observations in the holosteans longnose gar (*Lepisosteus osseus*) and the bowfin (*Amia calva*) (*35*, *36*) indicate that bilateral visual projections likely are ancestral among actinopterygians and arose before their diversification and that the ipsilateral component likely was subsequently lost in clupeocephalans. To further test this hypothesis, we analyzed visual projections in the Australian lungfish (*Neoceratodus forsteri*) a basal member of the lobe-finned fishes (Sarcopterygians) the monophyletic group that includes tetrapods. Lobe-finned fishes diverged from ray-finned fishes about 450 Ma and lungfish are now considered the closest living fish relative of tetrapods (*17*). In all injected animals (n=6/6) a small ipsilateral projection was found innervating the optic tectum (**Fig. 2, O** to **S** and **movie S3,** n=6). In contrast to other fish species analyzed here, ipsilateral projections intermingled with contralateral ones (**Fig. 2, R** and **S**; n=6). This was consistent with an earlier analysis of a single specimen of Australian lungfish (*37*) and supports the existence of bilateral visual projections in the bony vertebrate ancestor of actinopterygians and sarcopterygians (**fig.S1**). This intermingling of ipsilateral and contralateral axons could have some functional implications as it suggests that some tectal neurons might receive and integrate inputs from both eyes. Alternatively, it could represent an immature stage of visual system development that could be resolved in adult animals in an activity-dependent manner as it is the case in mammals. Together, these results indicate that the bilateral organization of the visual system likely did not appear in amniotes but that it is an ancestral vertebrate feature that emerged much earlier in evolution, before water-to-land transition and aerial vision adaptation in tetrapods.

Zic2 expression in the ipsilateral human embryonic retina

Our results raised questions about the evolution and conservation of the genetic mechanisms underlying visual system binocularity. Are they conserved in ray-finned fish with bilateral visual projections? The zinc-finger transcription factor Zic2 specifies the ipsilateral identity of ganglion cells in developing mice, ferrets and Xenopus (*5*). In Xenopus, Zic2 is absent from the neural retina of pre-metamorphic tadpoles that have only crossed visual projections, but Zic2 is expressed in ipsilaterally projecting ganglion cells after metamorphosis (*5*). To further evaluate and support the implication of Zic2 in the control of mammalian ganglion cell laterality, we analyzed the expression of ZIC2 in the human eye and compared it to mice by performing immunohistochemistry in whole-mount retinas. In human embryos, ganglion cell axons reach the brain by the 7th post-conception week (pcw7) and the optic nerve is well formed at pcw10 (*38*). Using the EyeDISCO clearing protocol (*15*) in mice, we observed that at embryonic day 16 (E16), the peak of Zic2 expression in mice (*5*), the retinal domain positive for Zic2 represented about 5.34±0.36 % of the total retinal surface (**Fig. 3, A** to **C** and **fig. S3A**; n=6 eyes). Post-mitotic ganglion cells, the first neurons generated in the retina(*39*), migrate to the basal side to accumulate at the inner surface of the retina and express the transcription factors Islet1 (*40*) and RNA-binding protein with multiple splicing (RBPMS)(*41*) (**Fig. 3**). At pcw9, RBPMS+ and ISLET1+ ganglion cells were present all over the retina (**Fig. 3, D** to **I**). Flat-mounted and sections of human retinas from pcw9 embryos, an age equivalent to E16 in mice (*40*), showed that ZIC2+ cells were restricted to the temporal quadrant of the retina (representing about 18.95±0.98 % of the retina surface), which contains ipsilaterally projecting ganglion cells in primates (**Fig. 3, D** to **J** and **movie S4**; n=3 eyes). ZIC2+ were ganglion cells as they co-expressed ISLET1 and RBPMS (**Fig. 3, F** to **H**). In the temporal retina, the density of ZIC2+/ISLET1+ ganglion cells was higher close to the ciliary marginal zone, at the edge of the retina (**Fig. 3G**), than in more medial regions where it was absent from the most superficial ISLET1+ (Fig. **3H** and **fig. S3B**) and RBPMS+ ganglion cells (**Fig. 3F and fig. S3**). ZIC2 was not detectable in the nasal retina (**Fig.3, D**, **E** and **I**). Unlike in the mouse (*42*), ZIC2 was not present in the neuroblastic layer which contains SOX2 (sex determining region Y-box 2) + progenitors (**Fig. 3, J** to **L** and **fig. S3C**). At pcw14, at the end of ganglion cell neurogenesis

(*39*), ZIC2 was still only present in the temporal retina (**Fig.3, K** and **L**). Although we could not access later stages of development, the absence of ZIC2 from the most superficial ganglion cells in the inner retina suggest that human ZIC2 is expressed in recently differentiated ipsilateral ganglion cells in the temporal retina and might be down-regulated as they mature, as is the case in mice.

Zic2 is not expressed in differentiating ganglion cells in fish with bilateral visual projections

The pivotal role for Zic2 in the specification of an ipsilateral axonal growth program in mammals was also well correlated with the absence of transcripts of the two *zic2* co-orthologs (*zic2a* and *zic2b*, generated in the TGD) in zebrafish ganglion cells (*43*) (**fig. S4, A to C** and E to **G**). Double fluorescent *in situ* hybridization for *zic2b* and *atoh7* (a committed precursor marker) from 24 to 48 hours post fertilization confirmed that *zic2b* did not colocalize with differentiating *atoh7*+ ganglion cells. By contrast, and as reported for zic2 in the mouse (*44*), *zic2b* was detected in the ciliary marginal zone, (**fig. S4M**, n=3) which contains dividing progenitors and stem cells producing all retinal cell types, even in adult teleosts (*45*, *46*) (**fig. S4, H to L**; n=5).

The presence of an ipsilateral visual projection in the spotted gar, as extensive as that of mice, together with its well characterized genome and the accessibility of gar embryos (*32*, *47*), led us to evaluate the expression of *zic2* in the developing gar retina. We first analyzed the development of the gar visual system using whole-mount immunolabelling, iDISCO+ clearing and light-sheet microscopy (**Table S1**) (*15*). In the spotted gar, a few Islet1- immunoreactive ganglion cells were detected at 2-3 days post fertilization (dpf) (**Fig. 4, A** and **B** and **fig.S5C** and **movie S5**; n=5). At 6-7dpf, optic nerves could be observed and had reached the optic chiasm (**Fig. 4, C** and **D** and **movie S5**; n=5). Development is slower in gar than in zebrafish and it is temperature-dependent (*48*). The next 10 days of development are only characterized by changes in fin opercular and gill formation but not in eye morphogenesis (*48*). By 17-18dpf the retina contained many ganglion cells and the optic tract was well developed (**Fig. 4, E** to **G** and **movie S5**; n=5). The highly proliferative ciliary marginal zone could be identified by the presence of cells expressing the S-phase marker, proliferating cell nuclear antigen marker and overlapping with *zic2* expression, which was absent from neighboring post-mitotic Islet1+ ganglion cells (**Fig. 4, H** to **L**). At 2-3dpf and 6-7 dpf, *zic2* mRNA was detected in proliferating cells of the developing neuroretina and progressively became restricted to the ciliary marginal zone (**fig. S5, A** to **D**). Its paralogs, *zic1* and *zic5*, also enriched in ipsilateral ganglion cell in mice (*49*), were absent from the embryonic gar retina (**fig. S5, E** to **L**). These results show that neither Zic2, Zic1 nor Zic5, specify ipsilateral ganglion cells in the spotted gar, suggesting that *zic* genes might be dispensable for gar ipsilateral projections. By contrast, the presence of Zic2 in the ciliary marginal zone of fish and mammals suggests that Zic2 might have a function in retinal precursors that is evolutionarily conserved.

In mammals, Zic2 acts in part by activating the expression of the receptor tyrosine kinase EphB1 in ipsilateral axons (*8*, *50*), whose ligand ephrinB2, localized at the chiasm, prevents crossing (*7*). According to the lack of Zic2 in the gar ganglion cells, we did not detect *ephB1* mRNA in the developing retina and *ephrinB2* was absent from the chiasm (**fig. S5, M** to **W**).

Zic2 overexpression induces ipsilateral projections in zebrafish

In mice, *Zic2* overexpression in the retina, outside the ipsilateral domain, increases the proportion of ipsilaterally projecting ganglion cell axons (*50*). Therefore, we tested the hypothesis that despite its absence in fish ganglion cells, the forced expression of Zic2 in zebrafish ganglion cells could affect their axonal targeting. We used a human *ZIC2-T2A-GFP* overexpression construct to express ZIC2 and GFP in the zebrafish eye under the control of the *atoh7* promoter. Vertebrate Zic2 proteins are highly conserved (*51*), with 81.1% identity between Human ZIC2 and zebrafish Zic2a and more than 93% similarity in the zinc finger domain (**fig. S6**). To visualize the projections coming from ZIC2 overexpressing ganglion cells derived from a single eye, we removed one eye at 2 dpf. As previously reported, under normal conditions retinal fibers from the remaining eye projected exclusively to the contralateral tectum (**Fig. 4, M** and **N**; n=10) (*52*, *53*). In contrast, ZIC2-expressing ganglion cells generated ipsilateral retinotectal afferent fibers representing a mean of 19.6±8.5% of the GFP+ axons (**Fig. 4, O** and **P**; n=10/13). Expression of *ZIC2* did not seem to bias the targeting of ganglion cell axons to their topographic position as previously reported in mouse (*54*). These results show that *zic2*, although not normally expressed in zebrafish ganglion cells, can still specify an ipsilateral program. In mice, the receptor tyrosine kinase EphB1 is expressed by ipsilateral ganglion cell axons and the ectopic expression of Zic2 in the contralateral retina induces EphB1 and reduce midline crossing at the chiasm (*8*, *50*). However, we could not detect EphB1 protein or mRNA (**fig. S7**) in zebrafish ganglion cells, neither in controls injected with GFP (n=13) nor in ZIC2-overexpressing fish (n=11) suggesting that these may be guided by alternative cues.

Discussion

It has been proposed that the evolution of terrestrial vertebrates followed an increase of eye size in aquatic vertebrates able to see through air, in a process that has occurred also in modern crocodiles or fish species similar to the four-eye fish and mudskippers (*55*). The existence of ipsilateral projections in the most basally branching groups of both actinopterygians and sarcopterygians indicates that ipsilateral connections were likely already present in the common ancestor of bony vertebrates, a bony fish, thus preceding aerial vision adaptation of tetrapods. This example highlights how the comparative study of a variety of species outside the list of the classical model species allows drawing evolutionary conclusions that may otherwise remain

obscured (*56*). Moreover, all the teleosts species analyzed in our study can be described as diurnal predators that heavily rely on visual cues to detect and consume their preys. These preys may vary in size from large vertebrates (redeye piranha) to small invertebrates (Mexican tetra, zebrafish, green-spotted puffer, Atlantic mudskipper and the four-eyed fish). In all cases our data show that ipsilateral projections in teleosts are not required for a visually mediated predatory behavior as it is usually assumed in mammals. Recent studies have confirmed this also in larval zebrafish where possible alternative neuronal circuits have been described (*53*).
On the other hand, lungfish and some basally branching actinopterygians, where ipsilateral projections are present, show reduced visual system development, as they are bottom dwellers that show nocturnal predatory behavior (lungfish and bichir) or feed on benthic organisms (sturgeon). Overall, our data show that the presence of ipsilateral projections in the visual system of fishes appears to correlate with phylogeny and not with life style or predatory behavior. Along these lines, it is therefore unlikely that ipsilateral retinal projections serve a function similar to what is commonly considered in mammals. On the contrary, visual system bilaterality might have been used as the neural substrate to compute stereopsis following the acquisition in diurnal mammals of visual-based predatory abilities after the Cretaceous–Paleogene (K–Pg) extinction event. Supporting this view, the number of ipsilateral projections in reptiles (chelonians and squamates) correlates neither with eye position nor with the degree of binocular field (*11*, *57*). It has been hypothesized that ipsilateral ganglion cells facilitate motor coordination by providing a direct visual feedback to the limb steering brain centers (*6*). However, the function of ipsilateral ganglion cells in fish remains elusive and behavioral studies in non-canonical model species such as the gar will be required to address this question.
The conservation of the main families of axon guidance cues and receptors in Bilateria suggested that the mechanisms underlying the development of neuronal connectivity are evolutionarily conserved (*58*, *59*). However, the loss of the gene encoding Deleted in Colorectal

Cancer receptor in some bird species (*60*) and the uniqueness of the Roundabout3 receptor in mammals (*61*) have challenged this view. Here we show that the guidance program specifying visual axon ipsilaterality does not appear to be entirely conserved as we failed to detect expression of a *zic2* and other *zic* genes or *ephB1* in spotted gar ganglion cells. Hence, the textbook model of Zic2 and EphB1 in orchestrating retinal ganglion cell laterality does not simply translate to fish. In rodents, the contralateral identity of ganglion cells is specified by *Islet2* (*62*) and *SoxC* (*63*) transcription factors but whether they influence the development of visual axons in fish is unknown. Therefore, further experiments are needed to address the molecular mechanisms underlying visual bilaterality in bony fish species. Are there other pathways, apart from Zic2, that could direct ipsilateral projections or which could block the contralateral fate that occurs normally? A recent study (*64*) shows that in mice, contralateral ganglion cells activate a non-canonical Wnt signaling pathway to cross the midline. In ipsilateral ganglion cells, Zic2 prevents midline crossing by inducing a genetic module that changes the expression of a set of genes to jointly inhibit this non-canonical Wnt pathway.

In fact, the ectopic expression of human ZIC2 in the developing zebrafish retina still induces the formation of ipsilateral visual axons without causing other targeting defects. This finding suggests a possible conservation in fishes of downstream components of the genetic program specifying ipsilateral axons in mammals although the factor initiating its expression and its relationship to Zic2 remains unclear in the gar and in other non-teleost fish. By parsimony principle, given our data, we propose that the presence of ipsilaterality in the bony vertebrate ancestor is the most likely explanation. In particular, the Australian lungfish data show that ipsilateral projections were likely present in the sarcopterygian fish ancestor of tetrapods. Lungfish also functions as outgroup to the actinopterygians and thereby making an independent origin of ipsilateral visual axons within actinopterygians a less likely hypothesis. An alternative, yet less parsimonious explanation, could be that ipsilaterality has evolved independently multiple times among bony vertebrates, using different genetic mechanisms.

References

1. S. Ramón y Cajal, *Histologie du système nerveux de l'homme & des vertébrés* (Maloine, Paris, 1909).
2. G. L. Walls, *The vertebrate eye and its daptative radiation* (Hafner Publishing company, Bloomfield Hills Michigan, 1942).
3. K. Mogi *et al.*, Optic chiasm in the species of order Clupeiformes, family Clupeidae: Optic chiasm of Spratelloides gracilis shows an opposite laterality to that of Etrumeus teres. *Laterality*. **14**, 495–514 (2009).
4. G. Jeffery, L. Erskine, Variations in the architecture and development of the vertebrate optic chiasm. *Prog. Retin. Eye Res.* **24**, 721–753 (2005).
5. E. Herrera *et al.*, Zic2 Patterns Binocular Vision by Specifying the Uncrossed Retinal Projection. *Cell*. **114**, 545–557 (2003).
6. M. L. Larsson, Binocular vision, the optic chiasm, and their associations with vertebrate motor behavior. *Front. Ecol. Evol.* **3**, 89 (2015).
7. S. Nakagawa *et al.*, Ephrin-B regulates the Ipsilateral routing of retinal axons at the optic chiasm. *Neuron*. **25**, 599–610 (2000).
8. S. E. Williams *et al.*, Ephrin-B2 and EphB1 Mediate Retinal Axon Divergence at the Optic Chiasm. *Neuron*. **39**, 919–935 (2003).
9. A. Seth *et al.*, Belladona/(lhx2) is required for neural patterning and midline axon guidance in the zebrafish forebrain. *Development*. **133**, 725–735 (2006).
10. C. P. Heesy, Seeing in stereo: The ecology and evolution of primate binocular vision and stereopsis. *Evol. Anthropol.* **18**, 21–35 (2009).
11. R. Ward, J. Repérant, S. Hergueta, D. Miceli, M. Lemire, Ipsilateral visual projections in non-eutherian species: random variation in the central nervous system? *Brain Res. Rev.* **20**, 155–170 (1995).
12. C. Saleeba, B. Dempsey, S. Le, A. Goodchild, S. McMullan, A Student's Guide to Neural Circuit Tracing. *Front. Neurosci.* **13**, 897 (2019).
13. W. L. Conte, H. Kamishina, R. L. Reep, The efficacy of the fluorescent conjugates of cholera toxin subunit B for multiple retrograde tract tracing in the central nervous system. *Brain Struct. Funct.* **213**, 367–373 (2009).
14. X. Luo *et al.*, Three-dimensional evaluation of retinal ganglion cell axon regeneration and pathfinding in whole mouse tissue after injury. *Exp. Neurol.* **247**, 653–662 (2013).
15. R. J. Vigouroux *et al.*, Revisiting the role of Dcc in visual system development with a novel eye clearing method. *Elife*. **9**, e51275 (2020).
16. L. C. Hughes *et al.*, Comprehensive phylogeny of ray-finned fishes (Actinopterygii) based on transcriptomic and genomic data. *Proc. Natl. Acad. Sci. U. S. A.* **115**, 6249–6254 (2018).
17. C. T. Amemiya *et al.*, The African coelacanth genome provides insights into tetrapod evolution. *Nature*. **496**, 311–316 (2013).
18. R. Betancur-R *et al.*, Phylogenetic classification of bony fishes. *BMC Evol. Biol.* **17**, 162 (2017).

19. R. O. Karlstrom *et al.*, Zebrafish mutations affecting retinotectal axon pathfinding. *Development*. **123**, 427–38 (1996).
20. E. Robles, E. Laurell, H. Baier, The Retinal Projectome Reveals Brain-Area-Specific Visual Representations Generated by Ganglion Cell Diversity. *Curr. Biol.* **24**, 2085–2096 (2014).
21. T. J. Voneida, C. M. Sligar, A comparative neuroanatomic study of retinal projections in two fishes: Astyanax hubbsi (the blind cave fish), and Astyanax mexicanus. *J. Comp. Neurol.* **165**, 89–105 (1976).
22. E. Fiebig, S. O. E. Ebbesson, D. L. Meyer, Afferent connections of the optic tectum in the piranha (Serrasalmus natteren). *Cell Tissue Res.* **231**, 55–72 (1983).
23. S. E. Ebbesson, H. Ito, B. R. Projections, Bilateral Retinal Projections in the Black Piranah (Serrasalmus niger). *Cell Tissue Res.* **213**, 483–495 (1980).
24. O. Jaillon *et al.*, Genome duplication in the teleost fish Tetraodon nigroviridis reveals the early vertebrate proto-karyotype. *Nature*. **431**, 946–957 (2004).
25. D. L. Meyer, E. Fiebig, S. O. E. Ebbesson, A note on the reciprocal connections between the retina and the brain in the puffer fish Tetraodon fluviatilis. *Neurosci. Lett.* **23**, 111–115 (1981).
26. L. N. Perez *et al.*, Eye development in the four-eyed fish Anableps anableps: Cranial and retinal adaptations to simultaneous aerial and aquatic vision. *Proc. R. Soc. B Biol. Sci.* **284** (2017), doi:10.1098/rspb.2017.0157.
27. A. B. Butler, W. M. Saidel, Retinal Projections in the Freshwater Butterfly Fish, Pantodon buchholzi (Osteoglossoidei). *Brain. Behav. Evol.* **38**, 127–140 (1991).
28. G. Lázár, S. Libouban, T. Szabo, The mormyrid mesencephalon. III. Retinal projections in a weakly electric fish, Gnathonemus petersii. *J. Comp. Neurol.* **230**, 1–12 (1984).
29. G. von der Emde *et al.*, Active electrolocation in Gnathonemus petersii: Behaviour, sensory performance, and receptor systems. *J. Physiol. Paris*. **102**, 279–290 (2008).
30. I. Braasch, J. H. Postlethwait, in *Polyploidy and Genome Evolution*, P. Soltis, D. Soltis, Eds. (Springer Berlin Heidelberg, 2012), pp. 341–383.
31. K. Du *et al.*, The sterlet sturgeon genome sequence and the mechanisms of segmental rediploidization. *Nat. Ecol. Evol.* **4**, 841–852 (2020).
32. I. Braasch *et al.*, The spotted gar genome illuminates vertebrate evolution and facilitates human-teleost comparisons. *Nat. Genet.* **48**, 427–437 (2016).
33. J. Repérant *et al.*, The Retinofugal Pathways in a primitive actinopterygian, the chondrostean Acipenser güldenstädti. An experimental study using degeneration, radioautographic and HRP methods. *Brain Res.* **251**, 1–23 (1982).
34. J. Repérant, J. P. Rio, D. Miceli, M. Amouzou, J. Peyrichoux, The retinofugal pathways in the primitive African bony fish Polypterus senegalus (Cuvier, 1829). *Brain Res.* **217**, 225–43 (1981).
35. R. G. Northcutt, A. B. Butler, Retinofugal pathways in the longnose gar Lepisosteus osseus (linnaeus). *J. Comp. Neurol.* **166**, 1–15 (1976).
36. A. B. Butler, R. G. Northcutt, Retinal Projections in the Bowfin, Amia calva: Cytoarchitectonic and Experimental Analysis. *Brain. Behav. Evol.* **39**, 169–194 (1992).
37. R. Glenn Northcutt, Retinal projections in the australian lungfish. *Brain Res.* **185**, 85–90 (1980).
38. J. M. Provis, D. Van Driel, F. A. Billson, P. Russell, Human fetal optic nerve: Overproduction and elimination of retinal axons during development. *J. Comp. Neurol.* **238**, 92–100 (1985).
39. Y. Lu *et al.*, Single-Cell Analysis of Human Retina Identifies Evolutionarily Conserved and Species-Specific Mechanisms Controlling Development. *Dev. Cell*. **53**, 473-491.e9

(2020).

40. A. Hoshino *et al.*, Molecular Anatomy of the Developing Human Retina. *Dev. Cell.* **43**, 763-779.e4 (2017).

41. J. M. K. Kwong, J. Caprioli, N. Piri, RNA Binding Protein with Multiple Splicing: A New Marker for Retinal Ganglion Cells. *Investig. Opthalmology Vis. Sci.* **51**, 1052 (2010).

42. Q. Wang, F. Marcucci, I. Cerullo, C. Mason, *eNeuro* **3**, ENEURO.0169-16.2016 (2016).

43. R. Toyama, D. M. Gomez, M. D. Mana, I. B. Dawid, Sequence relationships and expression patterns of zebrafish zic2 and zic5 genes. *Gene Expr. Patterns.* **4**, 345–350 (2004).

44. F. Marcucci *et al.*, The Ciliary Margin Zone of the Mammalian Retina Generates Retinal Ganglion Cells. *Cell Rep.* **17**, 3153–3164 (2016).

45. D. C. Otteson, A. R. D'Costa, P. F. Hitchcock, Putative stem cells and the lineage of rod photoreceptors in the mature retina of the goldfish. *Dev. Biol.* **232**, 62–76 (2001).

46. M. Fernández-Nogales, V. Murcia-Belmonte, H. Y. Chen, E. Herrera, The peripheral eye: A neurogenic area with potential to treat retinal pathologies? *Prog. Retin. Eye Res.* **68** (2019), pp. 110–123.

47. I. Braasch *et al.*, A new model army: Emerging fish models to study the genomics of vertebrate Evo-Devo. *J. Exp. Zool. B. Mol. Dev. Evol.* **324**, 316–41 (2015).

48. W. L. Long, W. W. Ballard, Normal embryonic stages of the longnose gar, Lepisosteus osseus. *BMC Dev. Biol.* **1**, 1–8 (2001).

49. Q. Lo Giudice *et al.*, Single-cell transcriptional logic of cell-fate specification and axon guidance in early-born retinal neurons. *Development.* **146**, dev178103 (2019).

50. C. García-Frigola, M. I. Carreres, C. Vegar, C. A. Mason, E. Herrera, Zic2 promotes axonal divergence at the optic chiasm midline by EphB1-dependent and -independent mechanisms. *Development.* **135**, 1833–1841 (2008).

51. J. Aruga, M. Hatayama, Comparative genomics of the Zic family genes. *Adv. Exp. Med. Biol.* **1046**, 3–26 (2018).

52. A. L. Dell, E. Fried-Cassorla, H. Xu, J. A. Raper, cAMP-Induced Expression of Neuropilin1 Promotes Retinal Axon Crossing in the Zebrafish Optic Chiasm. *J. Neurosci.* **33**, 11076–11088 (2013).

53. C. Gebhardt *et al.*, An interhemispheric neural circuit allowing binocular integration in the optic tectum. *Nat. Commun.* **10**, 5471 (2019).

54. C. García-Frigola, E. Herrera, Zic2 regulates the expression of Sert to modulate eye-specific refinement at the visual targets. *EMBO J.* **29**, 3170–3183 (2010).

55. M. A. MacIver, L. Schmitz, U. Mugan, T. D. Murphey, C. D. Mobley, Massive increase in visual range preceded the origin of terrestrial vertebrates. *Proc. Natl. Acad. Sci.* **114**, E2375–E2384 (2017).

56. G. Laurent, On the value of model diversity in neuroscience. *Nat. Rev. Neurosci.* **21**, 395–396 (2020).

57. S. Hergueta *et al.*, Overlapping visual fields and ipsilateral retinal projections in turtles. *Brain Res. Bull.* **29**, 427–433 (1992).

58. C. S. Goodman, The likeness of being: Phylogenetically conserved molecular mechanisms of growth cone guidance. *Cell.* **78**, 353–356 (1994).

59. P. Heger, W. Zheng, A. Rottmann, K. A. Panfilio, T. Wiehe, The genetic factors of bilaterian evolution. *Elife.* **9** (2020), doi:10.7554/eLife.45530.

60. F. Friocourt *et al.*, Recurrent DCC gene losses during bird evolution. *Sci. Rep.* **7**, 37569 (2017).

61. P. Zelina *et al.*, Signaling Switch of the Axon Guidance Receptor Robo3 during

Vertebrate Evolution. *Neuron*. **84**, 1258–1272 (2014).
62. W. Pak, R. Hindges, Y.-S. S. Lim, S. L. Pfaff, D. D. M. M. O'leary, Magnitude of Binocular Vision Controlled by Islet-2 Repression of a Genetic Program that Specifies Laterality of Retinal Axon Pathfinding. *Cell*. **119**, 567–578 (2004).
63. T. Kuwajima, C. A. Soares, A. A. Sitko, V. Lefebvre, C. Mason, SoxC Transcription Factors Promote Contralateral Retinal Ganglion Cell Differentiation and Axon Guidance in the Mouse Visual System. *Neuron*. **93**, 1110-1125.e5 (2017).
64. C. Morenilla-Palao *et al.*, A Zic2-regulated switch in a noncanonical Wnt/βcatenin pathway is essential for the formation of bilateral circuits. *Sci. Adv.* **6** (2020), doi:10.1126/sciadv.aaz8797.
65. I. Braasch et al., Connectivity of vertebrate genomes: Paired-related homeobox (Prrx) genes in spotted gar, basal teleosts, and tetrapods. *Comp. Biochem. Physiol. Part C Toxicol. Pharmacol.* **163**, 24–36 (2014).
66. V. Marillat et al., Spatiotemporal expression patterns of slit and robo genes in the rat brain. *J. Comp. Neurol.* **442**, 130–155 (2002).
67. C. Thisse, B. Thisse, High-resolution in situ hybridization to whole-mount zebrafish embryos. *Nat. Protoc.* **3**, 59–69 (2008).
68. V. Bercier et al., Dynactin1 depletion leads to neuromuscular synapse instability and functional abnormalities. *Mol. Neurodegener.* **14**, 27 (2019).
69. R. C. Edgar, MUSCLE: Multiple sequence alignment with high accuracy and high throughput. *Nucleic Acids Res.* **32**, 1792–1797 (2004).
70. F. Oteri, F. Nadalin, R. Champeimont, A. Carbone, BIS2Analyzer: A server for co-evolution analysis of conserved protein families. *Nucleic Acids Res.* **45**, 307–314 (2017).
71. D. Santos, S. M. Monteiro, A. Luzio, in *Methods in Molecular Biology* **1797**, 365–371 (2018).

Figure legends

Fig.1. Visual projections are only contralateral in clupeocephalan teleosts.

(**A**) Simplified phylogenetic tree of the major groups of vertebrates. Divergence of each major group is displayed in million years. Asterisks indicate whole genome duplication events in the teleost (TGD) and sturgeon (AGD) ancestors. (**B**) Whole brain visualization of a juvenile zebrafish injected with an AlexaFluor-555-conjugated CTb (left eye) and AlexaFluor-647-conjugated CTb (right eye) highlighting complete contralateral projections. (**C**) High magnification showing pre-tectal nuclei. (**D** to **M**) 3D rendering of visual projections labelled by injecting AlexaFluor-555-conjugated CTb (left eye) and AlexaFluor-647-conjugated CTb (right eye) followed by iDISCO whole-brain clearing and 3D imaging using light-sheet fluorescence microscopy. (D and E) Mexican tetra. (F and G) Redeye piranha. (H and I) Green-spotted pufferfish. (J and K) Four-eyed fish. (L and M) Atlantic mudskipper. In all species, visual axons only project to the brain on the contralateral side. Abbreviations: A, anterior; Cb, Cerebellum; Ctb, Cholera toxin B; D, dorsal; OB, Olfactory bulb; ON, Optic nerve; P, posterior; V, ventral; Sil, Silurian. Scale bars are 500 µm in (B) and (D) to (M) and 200 µm in (C).

Fig. 2. **Bilateral visual projections in basal ray-finned fishes and lobe-finned fishes**

(**A** to **S**) 3D light-sheet fluorescence microscopy images of iDISCO+ cleared brains from fish injected into the eyes with 2 cholera toxins. The left panels show only one channel. (**C, F, J, N** and **S**) are optical sections through the brain region receiving bilateral visual inputs. (**I** and **M** and **R**) high magnification from whole-mount brains. (A to C) Butterflyfish. (D to F) Spotted gar. (G to J) Sterlet sturgeon. (K to N) Armored bichir. (O to S) Australian lungfish. (C, F, J and N) In all fishes**,** contralateral and ipsilateral projections segregate in two different optic tectum (OT) layers except in the lungfish (S) where they are intermingled in the OT. Arrowheads indicate ipsilateral projections. Abbreviations: Cb, Cerebellum; OB, Olfactory bulb; OE, Olfactory epithelium; ON, Optic nerve; OC, Optic chiasm; pT, pretectal nuclei; T, Optic tract. Scale bars are 500 µm in (A, B, D, E, G, H, K, L, P and Q) and 80 µm in (C, G, K, N and S) and 100 µm in (M, O) and 150 µm in (I, R).

Fig. 3. Zic2 is expressed in the temporal retina of mammal embryos

(**A** to **C**) Whole-mount immunohistochemistry of an E16 mouse eye labeled with the pan ganglion cell marker RBPMS and the ipsilateral ganglion cell marker Zic2. (A) frontal view and (B) top view. (C) Optical section at the level indicated by the dashed line in (C). (**D** to **F**)**,** 3D light-sheet fluorescence microscopy of pcw9 human embryonic eye cleared using EyeDISCO and labeled for RBPMS and ZIC2. (D) frontal view and (E) top view. (F) Optical section at the level indicated by the dashed line in (C). G, H, I indicate the approximate positions of images in panels G-I. (**G** to **I**) retinal cryosections of a pcw9 human embryo eye labeled with ZIC2 and ISLET1 at 3 different levels: temporal and close to retinal outer limit (G), temporo-medial (H) and nasal (I). ZIC2 cells are in the ganglion cell layer (GCL) and co-express ISLET1. They are absent from the neuroblastic layer (NBL). (**J**) retinal cryosection of a pcw9 human embryo eye labeled with ZIC2 and SOX2. ZIC2 is absent from the NBL which contains SOX2+ progenitors. (**K** and **L**) retinal cryosections of a pcw14 human embryo eye labeled with ZIC2, SOX2 and ISLET1. ZIC2 is only present in ISLET1+ ganglion cells in the temporal retina and absent from SOX2+ progenitors (K). Abbreviations: D, dorsal ; V, ventral ; N, nasal ; T, temporal ; ON, optic nerve. Scale bars are 70 µm in (A and B) and 20 µm in (C) and 300 µm in (D and E) and 50 µm in (F to L).

Fig. 4. Zic2 is not expressed by ganglion cells in spotted gar and zebrafish

(**A** to **F**) Development of the visual system in the spotted gar. All images are 3D light-sheet fluorescence microscopy images of EyeDISCO-cleared spotted gar embryos labeled with Islet1 and acetylated Tubulin. (A and C and E) Top (dorsal) views of spotted gars at 2-3dpf (A), 6-7dpf (C), and 17-18dpf (E). (B and D and F) frontal views of whole spotted gar eyes at 2-3dpf (B), 6-7dpf (D), and 17-18dpf (F). The optic nerve (ON and asterisk) starts to form by 6-7dpf and is well developed by 17-18dpf. The optic chiasm (OC) is formed by 6-7dpf. (**G**) Coronal cryosection of spotted gar embryos at 17-18dpf labeled for ßIII-tubulin and Islet1. (**H** to **K)** cryosection from 17-18dpf spotted gar eyes hybridized with *zic2* riboprobe (H and J) and labeled for proliferating cell nuclear antigen (PCNA) and Islet1 (I, K and L). (**J** to **L**) higher magnification of the ciliary margin zone (area framed in I). (**M** to **P**) 3D rendering of whole-brain viewed from the top of zebrafish injected with Tg(*atoh7:Gal4,14UASubc:T2A-eGFP-pA*) (M and N) or *Tg(atoh7:Gal4,14UASubc:ZIC2-T2A-eGFP-pA* (O and P). N and P show segmented ganglion cell projections. (P) A large ipsilateral projection (arrowhead) is seen in the *Tg(atoh7:Gal4,14UASubc:ZIC2-T2A-eGFP-pA)*-injected fish. Abbreviations: ON, Optic nerve; OC, Optic chiasm; GCL, Ganglion cell layer; INL, Inner nuclear layer; ONL, Outer nuclear layer. Scale bars are 50 μm in (A, D, F, J, K, L, M to P) and 15 µm in (B) and 80 μm in (C, H and I) and 150 µm in (E) and 200μm in (G).

Acknowledgements

The authors wish to thank Anais Favre and Ali Abjaghou for assistance with light-sheet microscopy, Fabio Cortesi for help with lungfish experiments, Sylvie Dufour and all members of Alain Chédotal and Del Bene teams for helpful discussions and input during the project. We thank Sylvie Rétaux (Paris Saclay University) for help with Mexican tetra work and helpful comments on the manuscript. We thank Allyse Ferrara and Solomon David (Nicholls State University) and members of the Braasch Lab for help with gar work. **Funding:** Programme Investissements d'Avenir IHU FOReSIGHT (ANR-18-IAHU-01) (AC, FDB). INSERM cross-cutting program HuDeCA 2018 (AC). NIH R01OD011116 (IB). UQ Amplify Fellowship (RS).

Authors contribution: AC, FDB and RV designed the experiments. FDB, KD, KNBC, JV, SA, RV, PK, RS conducted the experiments. AC, KNBC and FDB obtained funding for the project. IB provided *Lepisosteus* samples and EH the human *ZIC2* cDNA. AC, FDB and RV designed the figures and wrote the manuscript. All authors discussed the results and commented on the manuscript. **Competing interests:** The authors declare no competing interests. **Data and materials availability:** All data are available in the manuscript or the supplementary materials.

List of supplementary materials

Materials and Methods
Figs. S1 to S7
Table S1
Movies S1 to S5

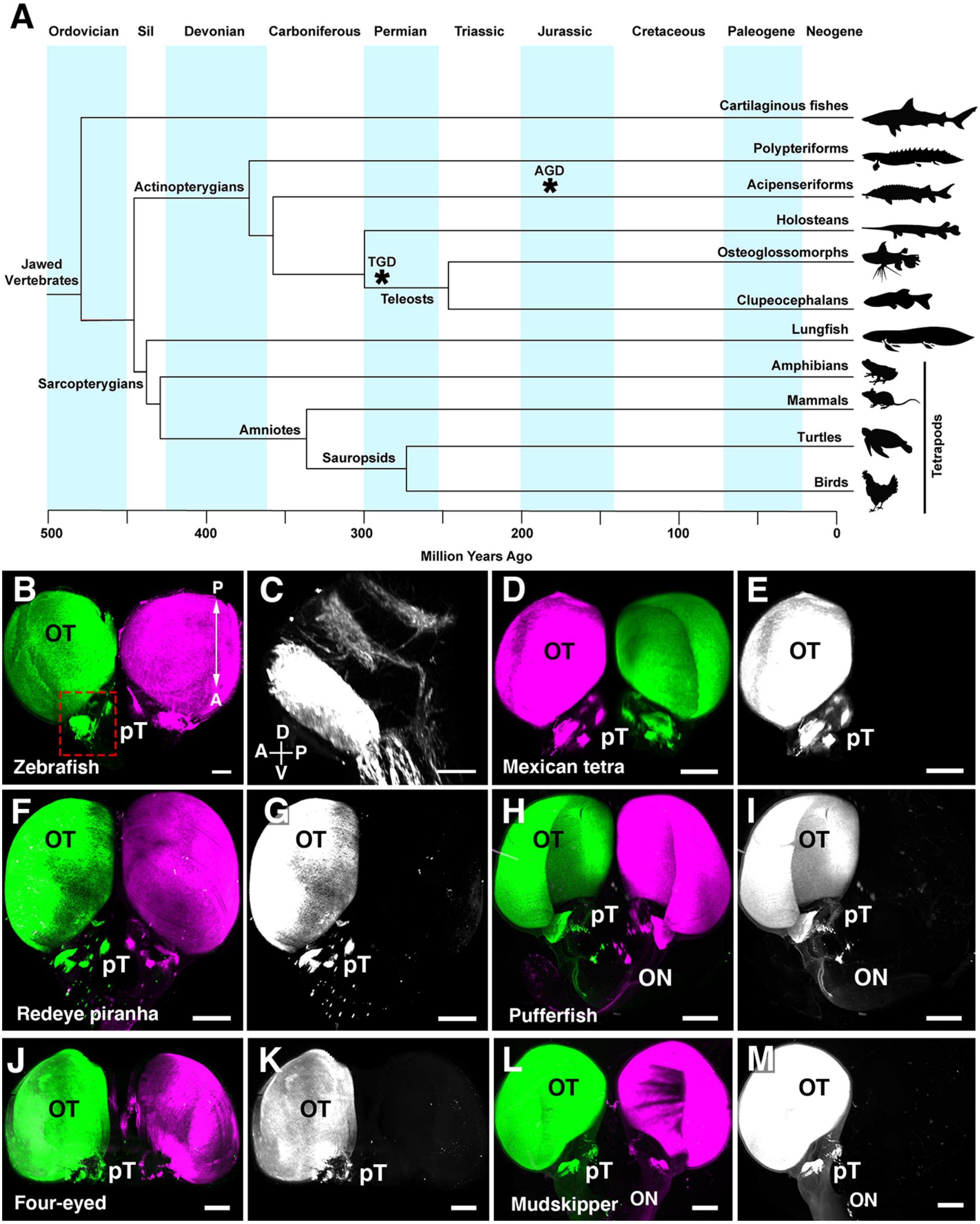

A
Ordovician
Sil
Devonian
Carboniferous
Permian
Triassic
Jurassic
Cretaceous
Paleogene
Neogene
Cartilaginous fishes
Polypteriforms
AGD
Acipenseriforms
Actinopterygians
Holosteans
Osteoglossomorphs
TGD
Jawed Vertebrates
Teleosts
Clupeocephalans
Lungfish
Amphibians
Sarcopterygians
Mammals
Amniotes
Turtles
Sauropsids
Birds
Tetrapods
500
400
300
200
100
0
Million Years Ago
B
OT
P
A
pT
Zebrafish
C
D
A
P
V
D
OT
pT
Mexican tetra
E
OT
pT
F
OT
pT
Redeye piranha
G
OT
pT
H
OT
pT
ON
Pufferfish
I
OT
pT
ON
J
OT
pT
Four-eyed
K
OT
pT
L
OT
pT
Mudskipper
ON
M
OT
pT
ON

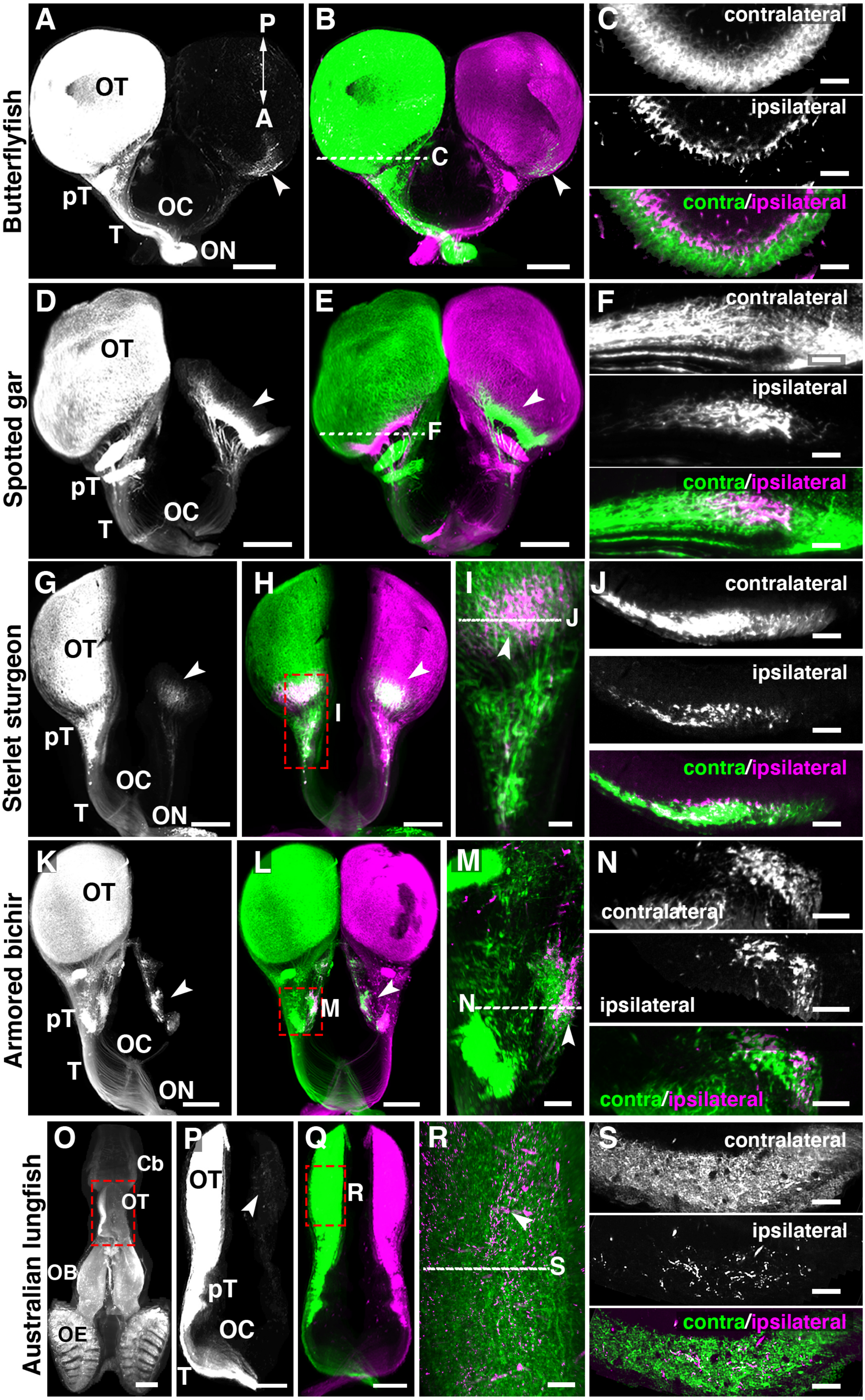

Butterflyfish
Spotted gar
Sterlet sturgeon
Armored bichir
Australian lungfish
A
P
A
OT
pT
T
OC
ON
B
C
contralateral
ipsilateral
contra/ipsilateral
D
OT
pT
T
OC
E
F
G
OT
pT
OC
T
ON
H
I
J
K
OT
pT
OC
T
ON
L
M
N
O
Cb
OT
OB
OE
P
OT
pT
OC
T
Q
R
S

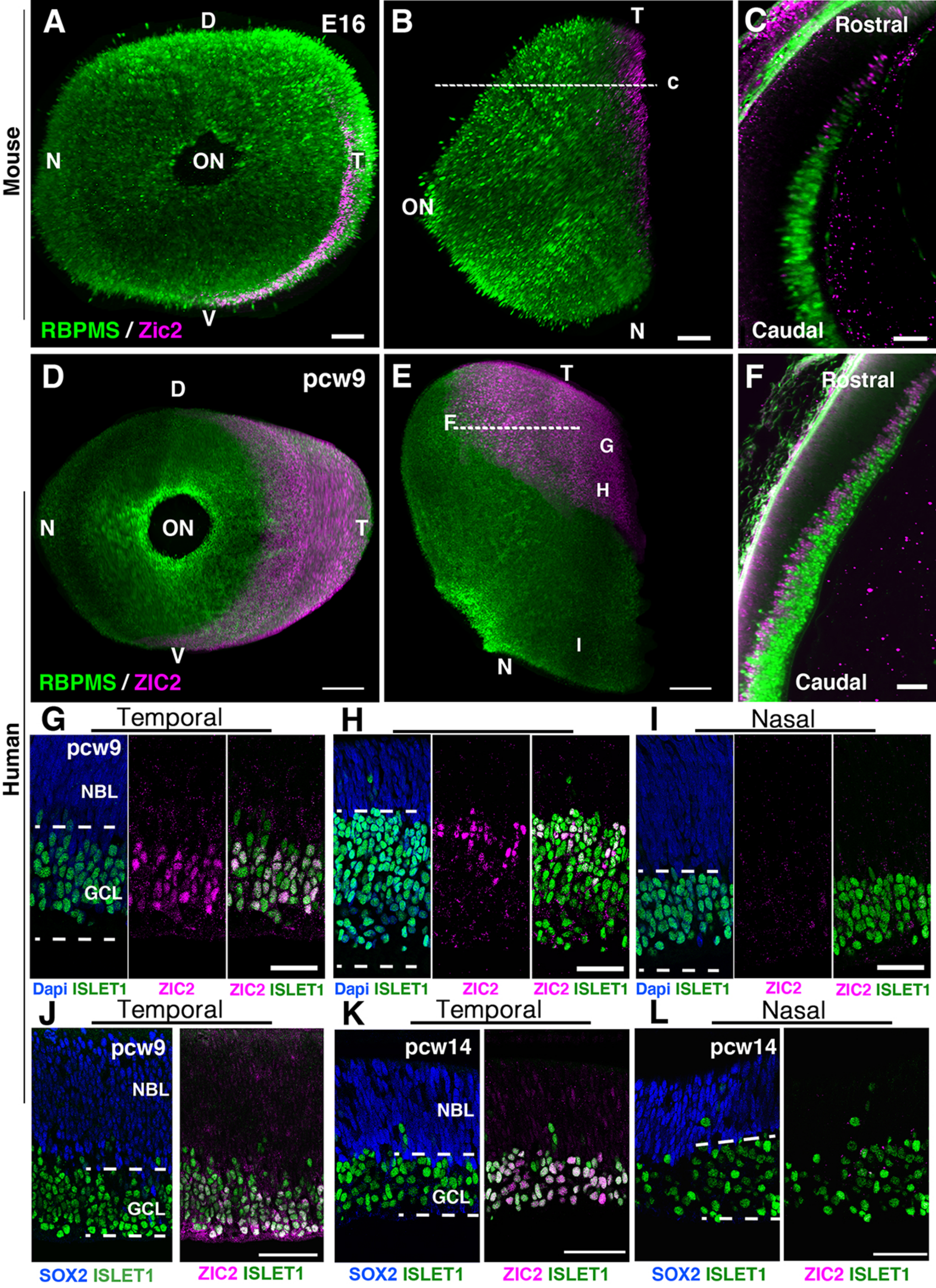

Mouse
Human
A
D
E16
N
ON
T
V
RBPMS / Zic2
B
T
c
ON
N
C
Rostral
Caudal
D
D
pcw9
N
ON
T
V
RBPMS / ZIC2
E
T
F
G
H
I
N
F
Rostral
Caudal
G
Temporal
pcw9
NBL
GCL
Dapi ISLET1
ZIC2
ZIC2 ISLET1
H
Dapi ISLET1
ZIC2
ZIC2 ISLET1
I
Nasal
Dapi ISLET1
ZIC2
ZIC2 ISLET1
J
Temporal
pcw9
NBL
GCL
SOX2 ISLET1
ZIC2 ISLET1
K
Temporal
pcw14
NBL
GCL
SOX2 ISLET1
ZIC2 ISLET1
L
Nasal
pcw14
SOX2 ISLET1
ZIC2 ISLET1

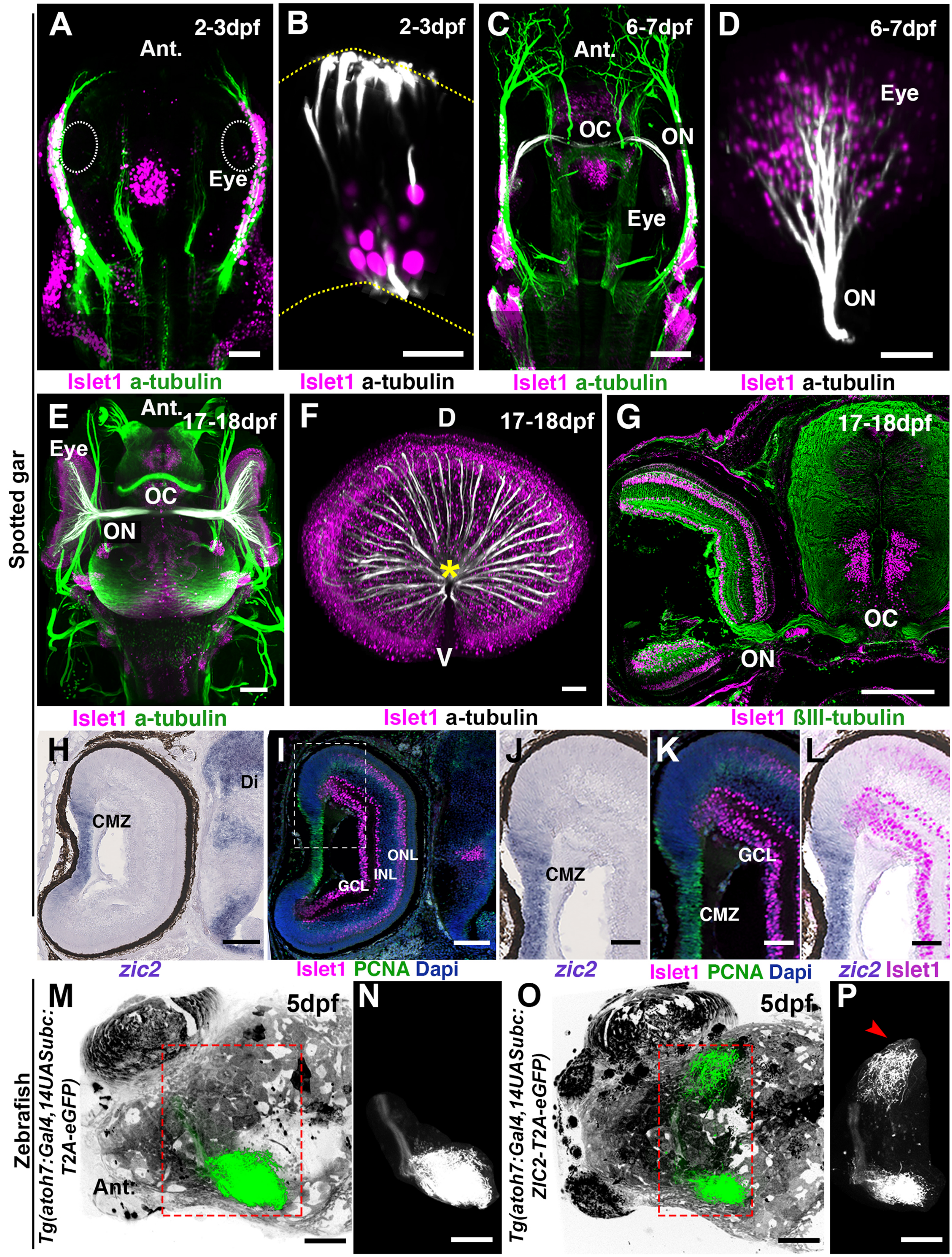
A
2-3dpf
Ant.
Eye
B
2-3dpf
C
6-7dpf
Ant.
OC
ON
Eye
D
6-7dpf
Eye
ON
Islet1 a-tubulin
Islet1 a-tubulin
Islet1 a-tubulin
Islet1 a-tubulin
E
Ant.
17-18dpf
Eye
OC
ON
F
D
17-18dpf
V
G
17-18dpf
OC
ON
Spotted gar
Islet1 a-tubulin
Islet1 a-tubulin
Islet1 ßIII-tubulin
H
Di
CMZ
I
ONL
INL
GCL
J
CMZ
K
GCL
CMZ
L
zic2
Islet1 PCNA Dapi
zic2
Islet1 PCNA Dapi
zic2 Islet1
M
5dpf
Ant.
N
O
5dpf
P
Zebrafish
Tg(atoh7:Gal4,14UASubc:T2A-eGFP)
Tg(atoh7:Gal4,14UASubc:ZIC2-T2A-eGFP)

Science
AAAS

Supplementary Materials for

Bilateral visual projections exist in non-teleost bony fish and predate the emergence of tetrapods

Robin J. Vigouroux, Karine Duroure, Juliette Vougny, Shahad Albadri, Peter Kozulin, Eloisa Herrera, Kim Nguyen-Ba-Charvet, Ingo Braasch, Rodrigo Suarez, Filippo Del Bene* and Alain Chédotal*

Correspondence to: filippo.del-bene@inserm.fr and alain.chedotal@inserm.fr

This PDF file includes:

Materials and Methods
Figs. S1 to S7
Table S1
Captions for Movies S1 to S5

Other Supplementary Materials for this manuscript include the following:

Movies S1 to S5

Material and Methods

Animals

Juvenile Mexican tetra (San Solomon Spring, Balmorhea State Park, Texas, USA) were maintained at 26°C (surface fish) on a 12:12 h light:dark cycle. Juvenile zebrafish and embryos were maintained at 28.5°C on a 14 h light/10 h dark cycle. Juvenile Australian lungfish (10.2-13.5 cm body length; Jardini Pty Ltd, Brisbane, Australia) were on freshwater at 26°C on a 12:12 h light:dark cycle. Juvenile armored bichir, sterlet sturgeon, African butterflyfish, redeye piranha, atlantic mudskipper, green puffer fish and four-eyed fish, were acquired from commercial vendors. Spotted gar embryos were spawned at Nicholls State University in Louisiana and then raised and maintained at Michigan State University as previously described (*65*). Embryos were raised at 18°C which leads to a comparatively slow progression through the Long & Ballard stages of gar development (*48*). Sizes of each specimen were recorded for future analysis. Juvenile specimens of either sex were used. All animal procedures were performed under the in accordance with protocols approved by Sorbonne Université and Institut Curie (EU0143-21323 and APAFIS #6031-2016070822342309), Queensland Brain Institute (#QBI/041/20/France) and Michigan State University (#10/16-179-00).

Human eye samples

Human fetal eyes from terminated pregnancies were obtained from the INSERM-funded Human Developmental Cell Atlas collection (HuDeCA, https://hudeca.genouest.org/). All tissues were collected with appropriate maternal consent and approval from the French National Biomedicine agency (N° PFS19-012).

In Situ Hybridization

Spotted gar sections were hybridized with digoxigenin-labeled riboprobes as described in (*66*). Briefly, tissue sections were postfixed for 10 min in 4% paraformaldehyde (PFA) before being treated with Proteinase K (10 µg/ml; Invitrogen, #03115852001) for 2 min and subsequently postfixed for 5 min in 4% PFA. Sections were then acetylated and permeabilized in PBS, 1% Triton X-100. Sections were first homogenized with hybridization buffer (50% formamide (VWR #24311.291), 5× SSC (Euromedex, #EU0300-A), 1× Denhardt's, 250 µg/ml yeast tRNA, and 500 µg/ml herring sperm DNA, pH 7.4) for 2 h at RT and then hybridized overnight at 72°C with riboprobes (1/200), see Table S1 for probe sequences. The next day, sections were rinsed for 2 h in 2× SSC at 72°C, and blocked in 0.1 M Tris, pH 7.5, 0.15 M NaCl (B1) containing 10% normal goat serum (NGS) for 1 h at RT. After blocking, slides were incubated o/n at 4°C with anti-DIG antibody conjugated with the alkaline phosphatase (1/5000, Roche Diagnostics) or anti-DIG antibody conjugated with peroxidase in B1 containing 1% NGS. After washing in B1 buffer, the alkaline phosphatase activity was detected by using nitroblue tetrazolium chloride (337.5 µg/ml) and 5-bromo-4-chloro-3-indolyl phosphate (175 µg/ml) (Roche Diagnostics). The peroxidase activity was detected by using Tyramide Signal Amplification (TSA) (PerkinElmer, #NEL741001KT) and incubated with Fluorescein fluorophore Tyramide diluted at 1:50 in TSA. Sections were mounted in Mowiol (Calbiochem/Merck, Carlstadt, Germany).

Whole-mount in situ hybridization were carried out on zebrafish as previously described (*67*). Embryos were then embedded in gelatin/albumin with 4% of glutaraldehyde and sectioned (20 μm) on a VT1000 S vibrating blade microtome (Leica). Slides were scanned with either a Nanozoomer (Hamamatsu) or laser scanning confocal microscope (Olympus, FV1000).

<u>Fluorescent in Situ Hybridization</u>

To generate anti-sense probes, DNA fragments were obtained by PCR using Phusion™ High-Fidelity DNA polymerase (Thermo Scientific, #F530L) with the primers listed in Table S1. Total cDNA from 1 to 5 dpf zebrafish were used as a template. PCR fragments were cloned into the pCRII-TOPO vector (Invitrogen, #K280040) according to manufacturer's instructions. All plasmids used were sequenced for confirmation. Anti-sense DIG or fluorescein-labeled riboprobes were *in vitro* transcribed using the RNA labeling kit (Roche, #11685619910 or #11277073910) according to manufacturer's instructions. De-chorionated embryos at the appropriate developmental stages were fixed in fresh 4% PFA in 1X PBS (pH7.4) containing 0.1% Tween20 (PBSTw) for 4 h at RT and stored o/n in 100% methanol. Embryos were re-hydrated by immersing them in subsequent baths of 50% methanol/PBSTw (Sigma, #34860) and then twice in PBSTw, baths followed by a 10 min incubation in a 3% H_2O_2/0.5%KOH (Sigma, #P5958) solution. Embryos were then rinsed in 50% methanol and post-fixed in 100% methanol at -20°C for 2 h. Embryos were then re-hydrated in methanol/PBSTw (75%/50%/25%) followed by treatment in 10 µg/ml proteinase K at RT (1 dpf = 5 min, 2 dpf = 15 min, 3 dpf = 20 min), and post-fixed for 20 min in 4% PFA in PBSTw. Embryos were pre-hybridized at 68°C, and hybridized with either a fluorescein-labelled probe or DIG-labelled probe or both probes for dFISH assays o/n at 68°C with gentle shaking. Embryos were then rinsed at 68°C in 50% formamide/2XSSC/0.1%Tween-20 twice, 2XSSC/0.1%Tween-20, 0.2XSSC/0.1% Tween-20 twice and finally in TNT buffer (0.1 M Tris pH7.5, 0.15 M NaCl, 0.1% Tween-20). Blocking was done in TNB buffer (2% DIG block (Roche, #11096176001) in TNT) for 2 h at RT and incubated o/n with anti-Fluo-Fab-POD (Roche, #11426346910) diluted at 1:50 in TNB buffer at 4°C. All steps were performed in the dark. Embryos were then washed several times in TNT, rinsed using 100 μl Tyramide Signal Amplification (TSA) (PerkinElmer, #NEL741001KT) and incubated with Fluorescein fluorophore Tyramide diluted at 1:50 in TSA.

The reaction was stopped by 5 rapid washes of TNT. For dFISH assays, the DIG-labelled probe was then revealed by carrying out a 20 min incubation in 1%H_2O_2/TNT (Sigma, #18312-1L), then washed several times in TNT. A second blocking step was carried out for 1 h in TNB buffer prior to incubating embryos in anti-DIG-POD (Roche, #11207733910) diluted at 1:100 in TNB buffer o/n at 4°C. Revelation was done with Cy3 Fluorophore Tyramide solution (PerkinElmer, NEL#744001KT), washed with TNT and processed for imaging upon DAPI staining.

Molecular cloning

14xUAS:ubc-ZIC2-T2A-GFP-pA or *14xUAS:ubc-T2A-GFP-pA* were obtained via Gibson assembly using the *pT1UciMP Tol1* (Addgene, #62215) destination vector described by (*68*). *Tol1*mRNA was synthesized from the plasmid (Addgene, #61388) digested by NotI (NEB, #R3189S) and retro-transcribed with SP6 RNA polymerase (Roche, #10810274001). Human ZIC2 (*hZIC2*), *GFP*, and *T2A* were amplified via PCR from pCAG-hZIC2 and *pUAS:Cas9T2AGFP;U6:sgRNA1;U6sgRNA2* (Addgene, #74009) respectively using the NEBuilder HiFi DNA Assembly Cloning kit (NEB, #E5520). Appropriate sequences were inserted after the *UBC* intron of the *pT1UciMP Tol1* destination vector opened by restriction digest with NcoI-HF (NEB).

Alignment between the amino acid sequences of the Zic2 proteins zing finger domains

A multiple sequence alignment was performed for the region covering the ZIC2 zinc finger domains of NCBI Reference Sequence proteins of mouse (NP_033600), human (NP_009060) and zebrafish (ZIC2a NP_571633, ZIC2b NP_001001820), as well as for genome-predicted ZIC2 proteins the spotted gar (XP_006638968). The UniProtKB/Swiss-Prot curated zinc finger sequences of human ZIC2 (O95409) were used to delineate the domain positions within the alignment. Protein sequence alignment was performed using MUSCLE version 3.8.31 (*69*), the amino acid conservation at each aligned position visualised using BIS2Analyzer (*70*).

Eye enucleation

The transgenic line *Tg*(*atoh7:gal4-vp16*) (RRID: ZFIN_ZDB-GENO-130306-1) was used. Prior to eye enucleation, fish were selected for the atoh7 expression in green. At 2 dpf, eye enucleation was performed. The embryos were anesthetized in 0.004% tricaine MS222 in a 2% agarose gel solution (Life technologies, #16520050). One eye was surgically removed using a pulled capillary and mouth pipetting. Embryos were then transferred into fish medium (egg medium with penicillin/streptomycin (Life Technologies, #15140122) and 0.003% 1-phenyl-2-thiouera (Sigma, #189235) until 5 dpf, for whole-mount immunohistochemistry.

Immunohistochemistry

Cryosections

Spotted gar embryos were fixed by immersion in 4% PFA in 0.12 M phosphate buffer (VWR, 28028.298 and 28015.294), pH 7.4 (PFA) o/n at 4°C. Following three washes in 1XPBS, the samples were incubated in 10% sucrose (VWR, 27478.296) in 0.12 M phosphate buffer o/n at 4°C. The next day, samples were transferred to a 30% sucrose solution in 0.12 M phosphate buffer o/n at 4°C. Samples were then embedded in 0.12 M phosphate containing 7.5% gelatin (Sigma, 62500) and 10% sucrose, frozen in isopentane at -40°C and then cut at 16 μm with a cryostat (Leica, CM3050S). Sections were blocked in PBS containing 0.2% gelatin (VWR) and 0.25% Triton-X100 (PBS-GT) for 1 h at RT. Following the blocking, sections were incubated with primary antibodies (see Table S1) diluted in a PBS-GT solution o/n at RT. Following three washes in PBST (0.05% Trinton-X100) secondary antibodies coupled to the appropriate fluorophore (see Table S1) were diluted in PBS-GT and incubated for 2 h at RT. Sections were counterstained with Hoechst (Sigma, B2883, 1:1000) or DAPI (Life Technologies, D3571, 1/500). For PCNA staining, an antigen retrieval step was performed by boiling sections in a 1X Sodium Citrate solution pH 6.0 for 5 min using a microwave. This step was skipped when the samples were first used for an *in-situ* hybridization assay. Slides were scanned with either a Nanozoomer (Hamamatsu) or laser scanning confocal microscope (Olympus, FV1000).

Whole-mount Immunohistochemistry

Zebrafish whole-mount immunohistochemistry was adapted from (*61*). Briefly, embryos were fixed in 4% PFA diluted in PBS containing 0.1% Tween-20 (VWR, #0777-1L) (PBSTw) for 4 h at RT and stored o/n in 100% methanol. After re-hydration, embryos were incubated for 20 min at -20°C in already pre-chilled acetone (Sigma, #650501). The embryos were rinsed several times with PBSTw and blocked for 2 h in blocking solution (10% bovine serum albumin (BSA) (Euromedex, #04-100-812-C), 10% normal goat serum (LifeTechnologies, #1000C), 1% DMSO (Sigma Aldrich, #D8418) in PBSTw). The primary antibodies were incubated o/n at 4°C in 1% BSA, 1% normal goat serum, 0.1% DMSO in PBSTw according to the dilutions in Table S1. After several washes in PBSTw, the secondary antibodies were incubated o/n at 4°C. The next day, embryos were rinsed in PBSTw and processed for imaging.

Whole-mount immunostaining on spotted gar embryos was carried out as previously described (*15*). Briefly, embryos were depigmented in a solution of 11% H_2O_2 (VWR, 216763) at 70 rpm exposed to an 11W warm white Light-Emitting Diode (LED) (3000° Kelvin) for 1-3 days. Samples were then blocked and permeabilized before being incubated with the primary antibodies for 7 days at RT (see Table S1) in a solution containing: 0.5% Tirton-X100, 5% donkey normal serum, 20% Dimethyl Sulfoxide, 1XPBS, 0.1 g/L thimerosal. The samples were further labeled with secondary antibodies (see Table S1) for 2 days at RT under agitation.

Retinal flat-mounts

For retinal flat mounts, human eyes were harvested and fixed in 4% PFA, followed by three washes in 1XPBS. Eyes were then de-pigmented using the EyeDISCO protocol as previously described (*15*). For immunohistochemistry, retinas were permeabilized and blocked in a solution containing 0.5% Triton-X100, 5% donkey normal serum, 1XPBS, 0.1 g/L thimerosal for 1 day at RT under agitation. Primary antibodies (see Table S1) were diluted in a solution containing 0.5% Triton-X100, 5% donkey normal serum, 20% Dimethyl Sulfoxide, 1XPBS, 0.1 g/L thimerosal for 3 days at RT under agitation. The retinas were then washed for 1 day in PBST (1XPBS, 0.5% Triton-X100). The secondary antibodies (see Table S1) were diluted in the same solution as primary antibodies and left for 2 days. After washing retinas for 1 day, they were mounted on slides and imaged using a scanning confocal microscope (Olympus, FV1000).

Tracing of visual projections

All fish were anesthetized with 0,04% MS222, tricaine-methanesulfonate (Sigma, #E10521) diluted in fish water. Australian lungfish were anesthetized with 0.05% clove oil in fresh water. Injection of cholera toxin β subunit was carried out as described in (*15*). Briefly, using a capillary approximately 1μl of 2 μg/μl of Alexa Fluor-conjugated cholera toxin β subunit (Thermo Fischer, Alexa Fluor555-CTb C22843 and Alexa Fluor647-CTb C34778) was injected intravitreally. 72-96 h following CTb injection, specimens were transcardially perfused with 4%PFA and the heads and/or brains were dissected for tissue clearing.

Tissue clearing and imaging

Clearing

Prior to clearing, spotted gar *embryos* were embedded in 1.5% agarose (Roth) in 1X TAE (Life Technologies). Clearing was carried out as previously described (*15*). Briefly, samples were gently de-hydrated in ascending baths of methanol (1.5 h). Samples were further treated with a solution containing 2/3 Dichloromethane (DCM, Sigma) 1/3 methanol o/n. The next day, samples were placed in DCM for 30 min prior to being immersed in Di-benzyl Ether (DBE, Sigma).

Imaging

Acquisitions were performed by using an UltraMicroscope I (Miltenyi Biotec, Germany) or UltraMicroscope Blaze (Miltenyi Biotec, Germany) with the ImspectorPro software (Miltenyi Biotec, Germany, 5.1.328 version). The light sheet was generated by a laser (wavelength 488, 561, 647 Coherent Sapphire Laser, LaVision BioTec, Miltenyi Biotec, Germany) or a second-generation laser beam combiner (wavelengths 488 nm, 561 nm and 647 nm; LaVision BioTec, Miltenyi Biotec, Germany). All light sheets were matched within their Rayleigh lengths for optimal illumination at the sample site. Either a binocular stereomicroscope (Olympus, MXV10) with a 2x objective (Olympus, MVPLAPO) was used Or a MI Plan 1.1x (NA = 0.1), a MI Plan 4x (NA = 0.35), and a MI Plan 12x (NA = 0.53) objectives were used (Miltenyi Biotec, Germany). Samples were placed in an imaging reservoir made of 100% quartz (LaVision BioTec, Miltenyi Biotec) filled with DBE and illuminated from the side by the laser light. A Zyla sCMOS camera (Andor, Oxford Instrument; 2,048 × 2,048, 6.5 x 6.5 μm^2, peak QE 82%) was used to acquire images. The step size between each image was fixed at 1 or 2 µm (NA = 0.5, 150 ms time exposure). All tiff images are generated in 16-bit.

Confocal microscopy

Whole-mount 5 dpf zebrafish larvae were mounted in a labtex plates (LabTex) in 2.5% agarose or in 1% low-melting agarose on FluoroDish Cell Culture dish (FD3510-100, World Precision Instruments). For imaging, a scanning inverted confocal microscope (FV1200, Olympus) was used with a 30x objective (Olympus, UPLSAPO30XS, NA = 1.05, WD = 0.8 mm) as well as the LSM780 and LSM880 scanning inverted confocal microscopes (Zeiss) for high resolution microscopy. 40x water immersion objective for whole mount dFISH stained zebrafish embryos and 63x oil objective for zebrafish retinal cryosections were used and a 10x air objective was used to image the spotted gar cryosections.

Image Processing

3D rendering of light sheet and confocal stacks were converted to an Imaris file (.ims) using ImarisFileConverter (Bitplane, 9.5.1 version) and then visualized using the Imaris x64 software (Bitplane, 9.5.1). To quantify ipsilateral territories, entire tectum volume and ipsilateral projections were automatically segmented with a surface detail of 5.00 μm, automatic threshold. Volumes were extracted from the surface. Movies were generated using the animation tool on Imaris x64 software (Bitplane, version 9.1.2) and movie reconstruction with .tiff series were done using ImageJ (1.50e, Java 1.8.0_60, 64-bit). All movie editing (text and transitions) was performed using iMovie (Apple Inc., version 10.1.1).

To quantify the ipsilateral projections in the hZIC2 overexpression experiments, a fixed region of interest was identified for each zebrafish (corresponding to the ipsilateral and contralateral optic tecta). Retinal projections were segmented with a surface detail of 0.5 μm using an automatic threshold. Ipsilateral and contralateral volumes were extracted and summed to constitute the "total visual projections" using Imaris x64 software (Bitplane, version 9.1.2). The volume of ipsilateral projections was isolated as a ratio of ipsilateral projections:total projections.

Statistical analyses

All data are described are listed as biological replicates (n) and all experiments (N) were carried out at least in triplicates unless indicated otherwise). An observer blinded to the experimental conditions realized all the quantifications. No data were excluded from the statistical analyses. All data are represented as mean values ± SEM. Statistical significance was estimated using two-tailed unpaired tests for non-parametric tendencies (Kruskall-Wallis or Mann-Whitney), two-way ANOVA and Bonferroni's multiple comparison test. $* = p < 0.05$; $** = p < 0.01$; $*** = p < 0.001$, $*** = p < 0.0001$. All statistical measurements were carried out using GraphPad Prism 7.

Supplementary Figures

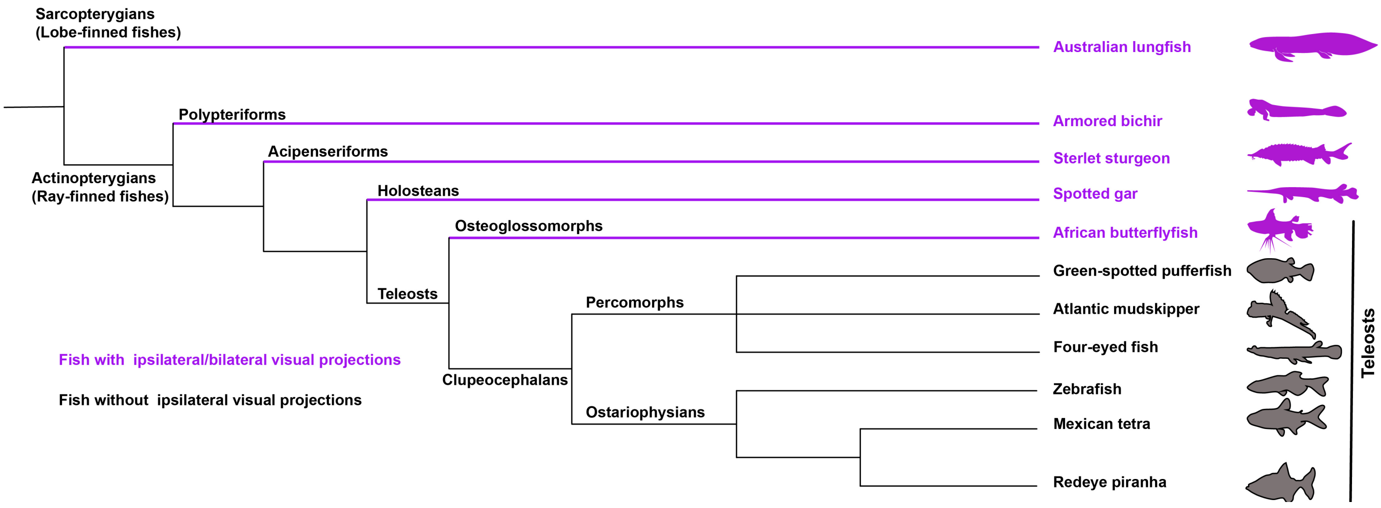

Fig. S1. Simplified chart of fish taxonomy indicating the species analyzed in this study.
Fish with bilateral/ipsilateral visual projections appear in magenta and fish with only contralateral visual projections appear in grey.

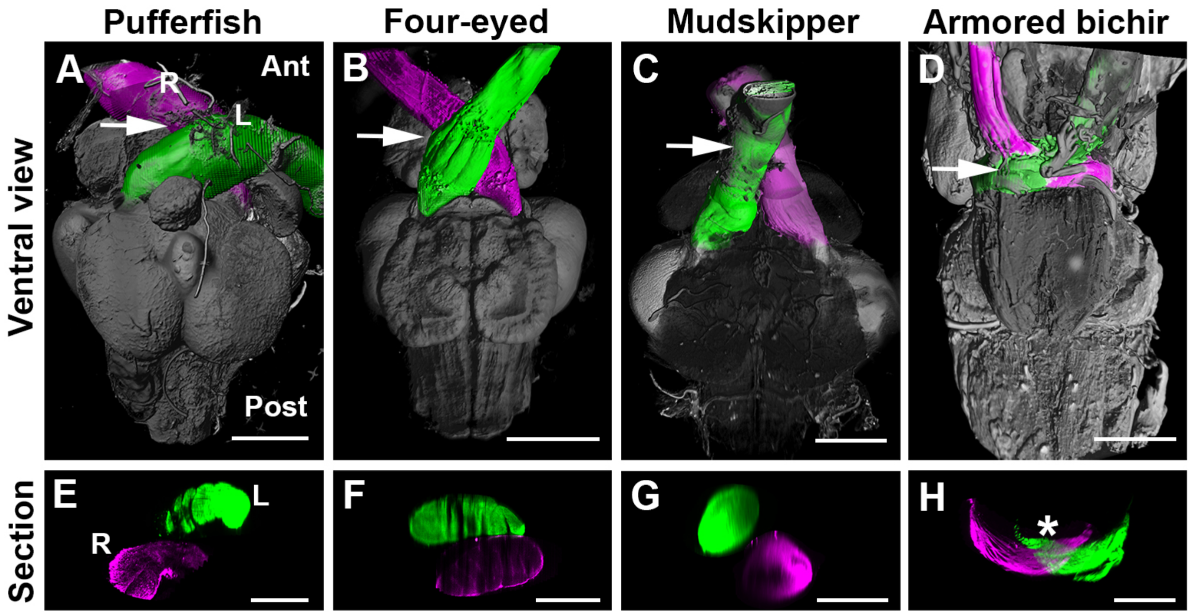

Fig. S2. Two types of optic nerve crossing modalities in ray-finned fishes.
Ventral views (**A** to **D**) and coronal optical sections (**E** to **H**) at the level of the optic chiasm of iDISCO-cleared brains and optic nerves. A surface rendering with normal shading (Imaris) was applied to generate the ventral view images. The arrowheads (A to D) indicate the level of the chiasm optical section in (E to H). In all fishes, one eye was injected with Alexa Fluor-555-conjugated CTb and the other one with Alexa Fluor-647-conjugated CTb. The right (R) and left (L) optic nerves were pseudo-colored in magenta and green respectively. In Pufferfish (A and E), Four-eyed (B and F) and Muskipper (C and G), the two optic nerves pass over and overlap at the chiasm but remain separated up to the brain. By contrast, in the Armored bichir (D and H), the right and left nerves meet at the chiasm and retinal ganglion cell axons from both eyes interweave during crossing (asterisk). Abbreviations: Ant, anterior; Post, Posterior. Scale bars are: 2 mm in (B), 1 mm in (A, C, D, F), 800 μm in (G), 600 μm in (E, H).

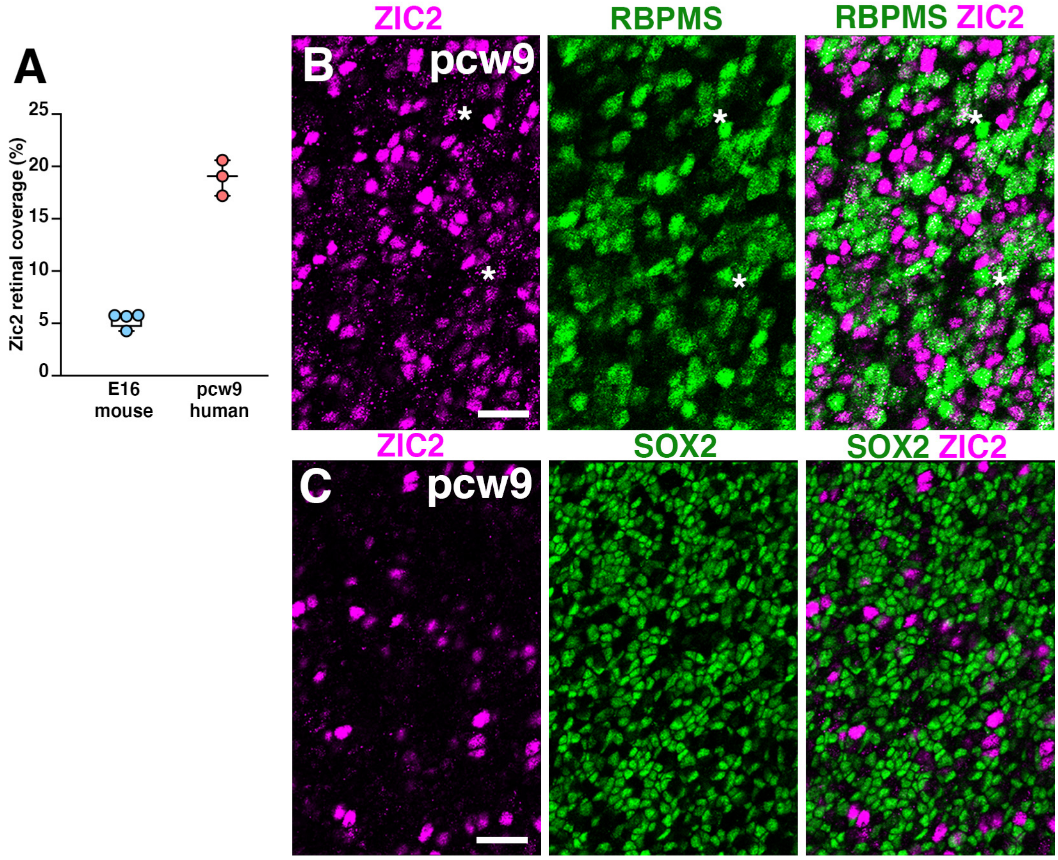

Fig. S3. ZIC2 expression pattern in human embryo retina.
(**A**) Box and whiskers representation of the ZIC2-positive surface in E16 mouse and pcw9 human retinas. (**B** and **C**) flat-mount pcw9 human retina labeled for ZIC2 and RBPMS (B) or SOX2 (C). (B) In the most superficial (basal side) regions of the temporal retina, ganglion cells expressing low levels of ZIC2 and RBPMS (arrowheads) are seen but ZIC2 and RBPMS are mostly exclusive. (C) image at the level of the interface between the neuroblastic layer showing that ZIC2+ cells are not SOX2+. Scale bars are: 50 μm in (B and C).

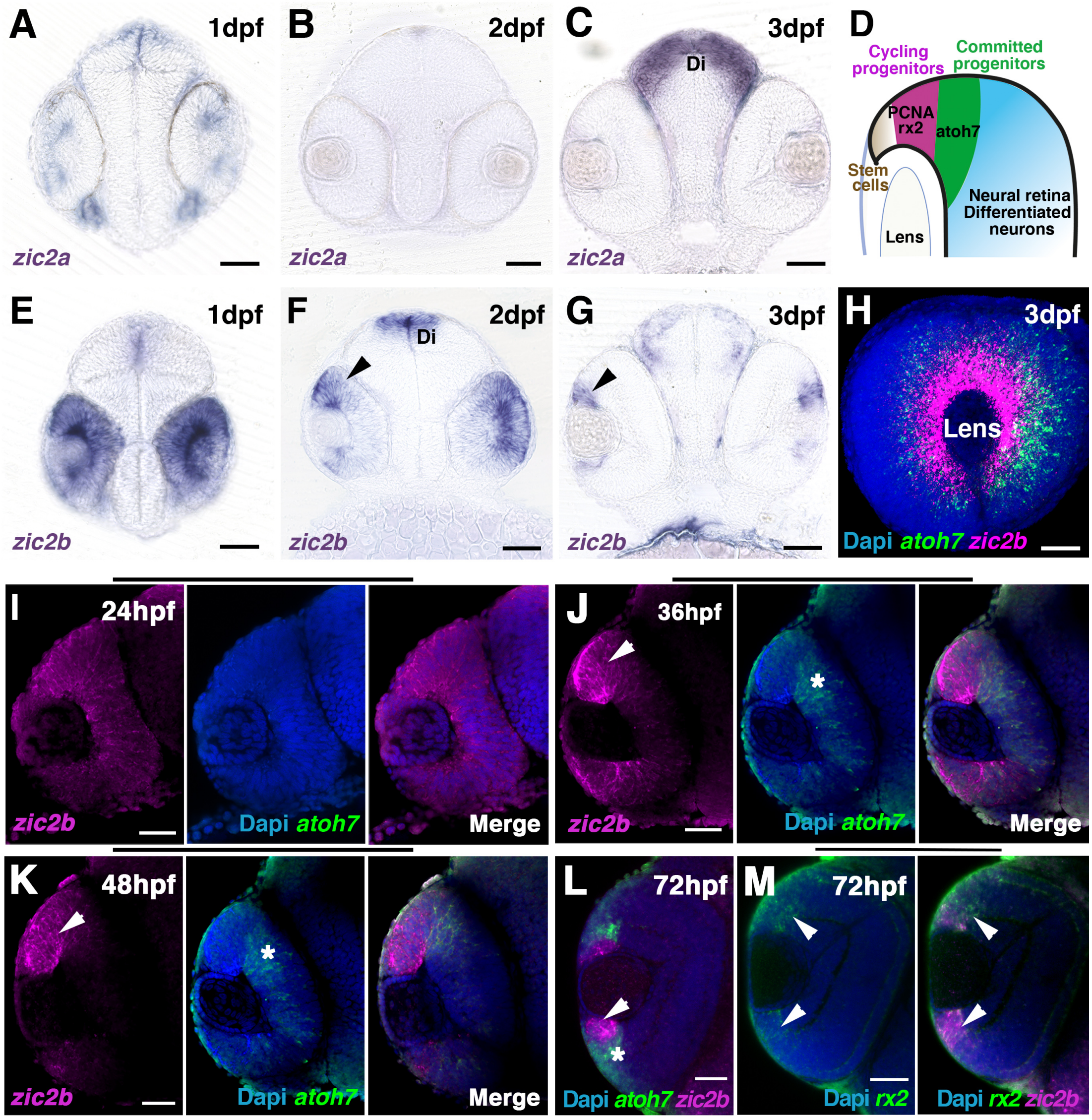

Fig. S4. Zic2 ortholog expression in zebrafish is restricted to the ciliary margin zone.
(**A** to **H**) Whole-mount *in situ* hybridization of zebrafish embryos for *zic2a* at 1 day post fertilization (1 dpf; A), 2 dpf (B) and 3 dpf (C) as well as *zic2b* at 1 dpf (E), 2 dpf (F) and 3 dpf (G). Zic2b is expressed in the ciliary marginal zone (CMZ, arrowheads in F and G) and in the dorsal diencephalon (Di). (D) Schematic drawing of the zebrafish CMZ in the developing retina showing spatial distribution of stem cells, cycling progenitors, committed progenitors and differentiated neurons. (H)**,** Lateral view of whole-mount double fluorescent *in situ* hybridization for *zic2b* and *atoh7* on 3 dpf zebrafish embryos with DAPI counterstaining. (I to L) Confocal sections through the central retina of wild-type embryos hybridized with antisense RNA probes for *zic2b* and *atoh7*. At 24 hpf, *zic2b* is expressed in the entire proliferative neuroepithelium and later from a central to peripheral wave-like manner (arrowheads) in complementarity to the neurogenic transient expression of *atoh7* (asterisks) as shown here for 36, 48 and 72 hpf. (L to M) Confocal sections through the central retina of 72 hpf wild-type zebrafish embryos hybridized with antisense RNA probes for *zic2b* and *retinal homeo- box transcription factor2* (*rx2*, a marker or dividing progenitors and stem cells in the CMZ). *Zic2b* expression overlaps with the expression of the *rx2* (arrowheads). All retinae were counterstained with the nuclear marker DAPI. Scale bars are 50 µm (A to C and E to H) and 40 µm (I to M).

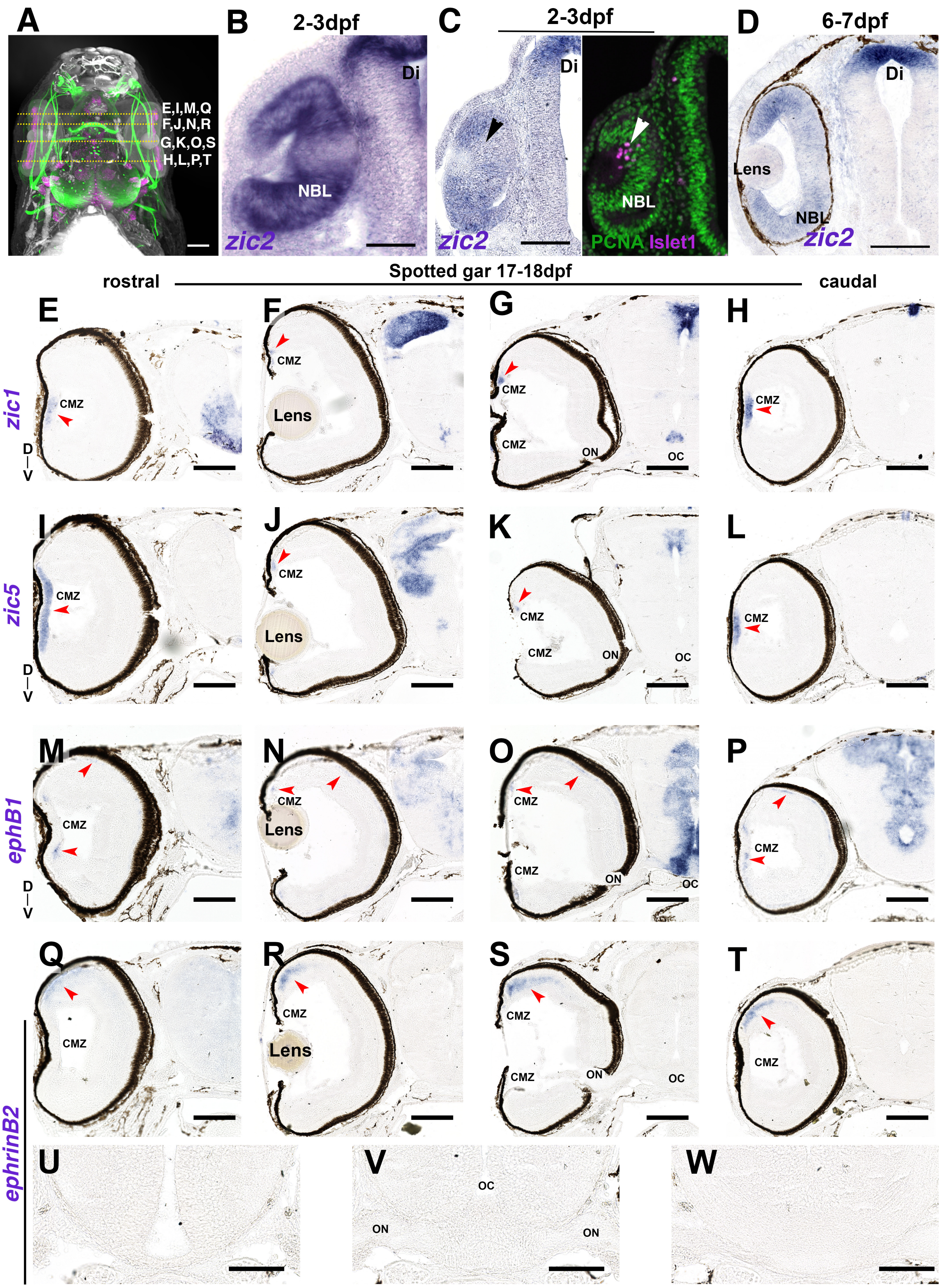
A
E,I,M,Q
F,J,N,R
G,K,O,S
H,L,P,T
B
2-3dpf
Di
NBL
zic2
C
2-3dpf
Di
zic2
NBL
PCNA Islet1
D
6-7dpf
Di
Lens
NBL
zic2
rostral
Spotted gar 17-18dpf
caudal
zic1
zic5
ephB1
ephrinB2
CMZ
Lens
ON
OC
D
V

Fig. S5. Mammalian ipsilateral markers are not expressed in the spotted gar visual system.

(**A**) 3D light-sheet fluorescence microscopy images of iDISCO-cleared 17-18 dpf spotted gar indicating with dotted lines the anatomical levels of the cryosections. (**B** to **D**) *In situ* hybridization for *zic2* on retinal cryosections of the developing spotted gar at 2-3 dpf (B), 6-7 dpf (C, left panel), 17-18 dpf (D). Only proliferating cells in the neuroblastic layer (NBL) express *zic2*. The right panel in (C) is an immunostaining for PCNA and Islet1. The arrowheads in (C) indicate the region where the first ganglion cells (Islet1+) are present at this stage in the retina. *zic2* is also found in the diencephalon (Di). (**E** to **T**) Rostral-to-caudal coronal cryosections from 17-18 dpf spotted gar. *zic1* (E to H) and *zic5* (I to L) are only expressed in the ciliary marginal zone (CMZ; arrow). (**M** to **P**) *ephB1* is absent from the retina and weakly expressed in the CMZ. (**Q** to **T**) *ephrinB2* is expressed in the dorsal retina (arrow). (**U** to **W**) Cryosections of the diencephalon of a 17-18dpf spotted gar hybridized for *ephrinB2*. *ephrinB2* is absent from the optic chiasm (asterisk). Immuno-reactive regions are highlighted (arrowhead). Abbreviations: NBL, Neuroblastic layer; ON, Optic nerve, OC, Optic chiasm; GCL, Ganglion cell layer; INL, Inner nuclear layer; ONL, Outer nuclear layer. Scale bars: A, 200 μm; B to D, 50 μm; C,U to W, 100 μm; D to T, 250 μm.

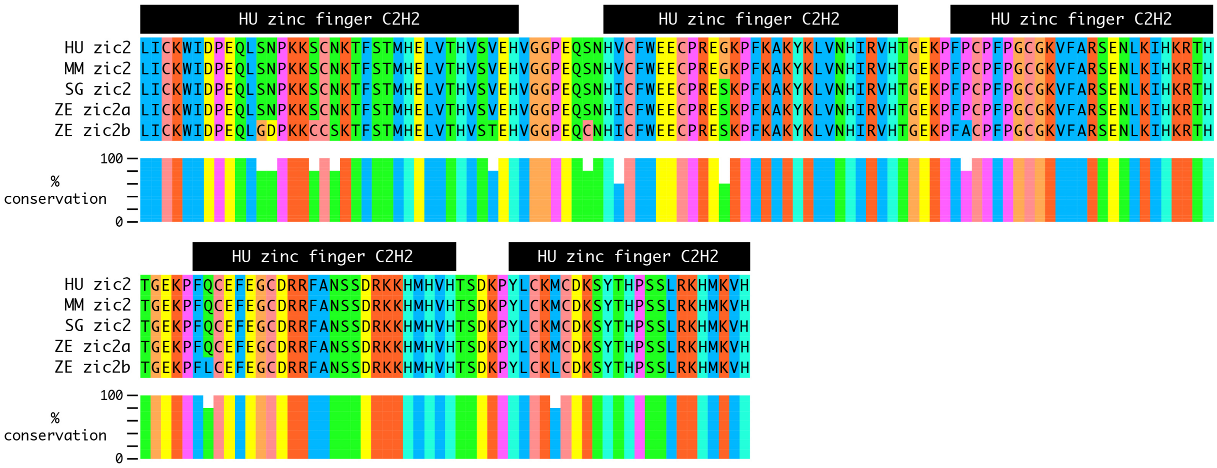

Fig. S6. Alignment between the amino acid sequences of the Zic2 protein zing finger domains of fish and mammals.

Alignment of Zic proteins across the zinc finger domains shows the high level of conservation between ray-finned fish and mammals. Amino acids are color coded according to the physiochemical class they belong to. Abbreviations: HU, human; MM, mouse; SG, spotted gar; ZE, zebrafish.

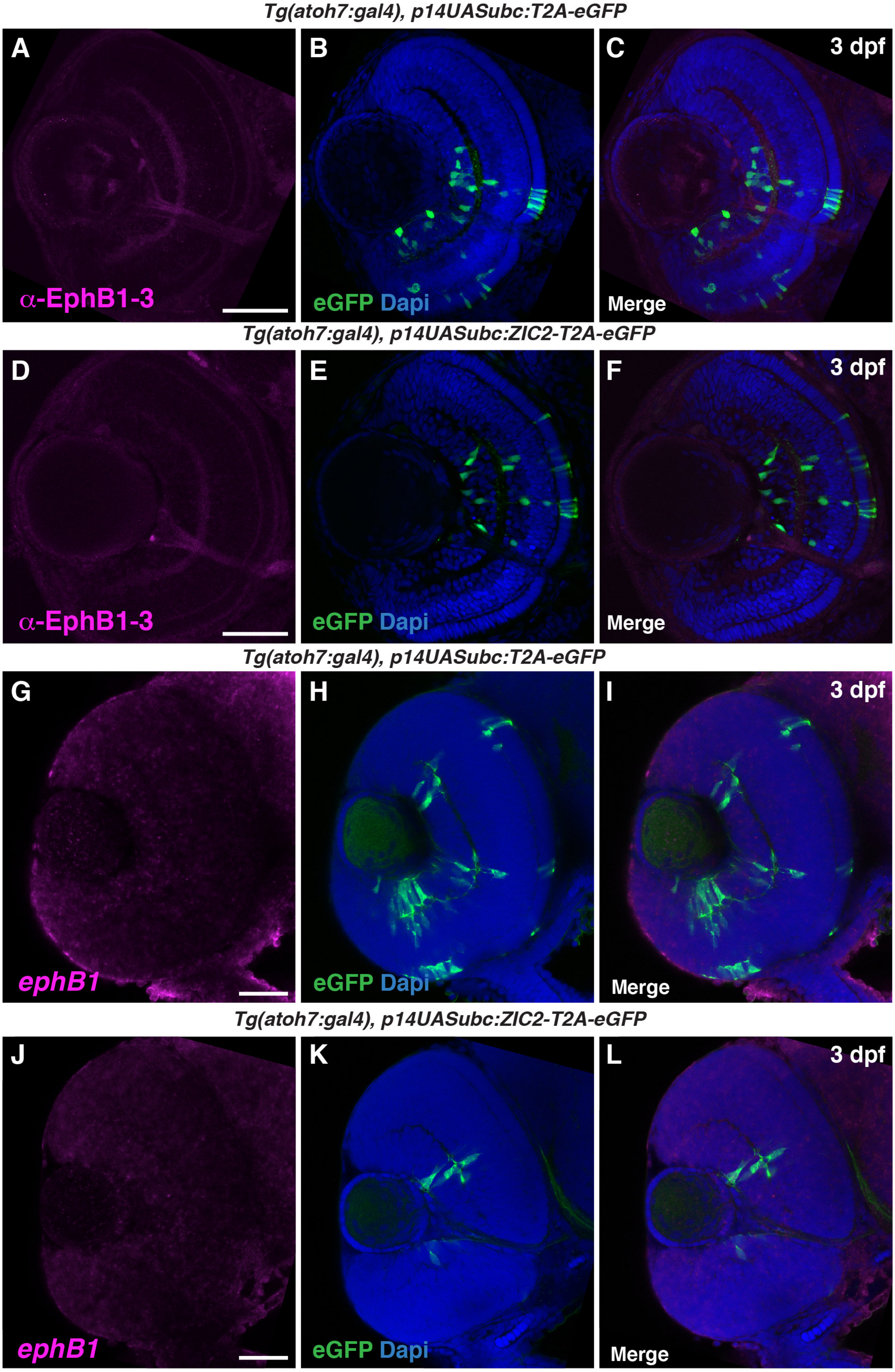
Tg(atoh7:gal4), p14UASubc:T2A-eGFP
A
B
C
3 dpf
α-EphB1-3
eGFP Dapi
Merge
Tg(atoh7:gal4), p14UASubc:ZIC2-T2A-eGFP
D
E
F
3 dpf
α-EphB1-3
eGFP Dapi
Merge
Tg(atoh7:gal4), p14UASubc:T2A-eGFP
G
H
I
3 dpf
ephB1
eGFP Dapi
Merge
Tg(atoh7:gal4), p14UASubc:ZIC2-T2A-eGFP
J
K
L
3 dpf
ephB1
eGFP Dapi
Merge

Fig.S7. Ectopic *ZIC2* expression in *atoh7* retinal progenitor cells does not induce EphB1 expression in retinal ganglion cells.

Confocal images of cryostat (**A-F**) or optical (**G-L**) sections of 3 dpf retinae from *Tg*(*atoh7:gal4*) embryos injected at 1-cell stage with either a *p14UASubc:T2A-eGFP* (A to C and G to I) control construct or a *p14UASubc:ZIC2-T2A-eGFP* construct (D to F and J to L). No signal for EphB1 in GFP-positive cells is detectable in all injected retinae either double stained with anti-EphB1 antibody (A to F) or hybridized with an *ephB1* antisense riboprobe (G to L). All retinae were counterstained with the nuclear marker DAPI. Scale bars are 50 μm.

Table S1. Comprehensive table summarizing the antibodies and probes sequences.

In situ probes						
Name	**Sequence**			**RRID**	**Dilution**	**In situ hybridization**
L-zic1 fwd	ACCTCCAGACATCACTCAAC			n/a	1:200	Cryosections
L-zic1 rev	GGAACACTCTTCCCAGAAAC			n/a	1:200	Cryosections
L-zic2 fwd	AAACTTAACCACGACCTCTCTC			n/a	1:200	Cryosections
L-zic2 rev	CTCGTGCATTGTGCTGAAAG			n/a	1:200	Cryosections
L-zic5 fwd	CTTTGAGCAAGAGGAATCCGGC			n/a	1:200	Cryosections
L-zic5 rev	CCTGCCGCGATGTTCACATTTA			n/a	1:200	Cryosections
L-efnb2 fwd	TCCCCATTATGAGAAGGTGAGCGG			n/a	1:200	Cryosections
L-efnb2 rev	ACAGGCTACCACTTCAGAAGGCAG			n/a	1:200	Cryosections
L-ephb1 fwd	AGAACCTGAACACAATCCGCAC			n/a	1:200	Cryosections
L-ephb1 rev	ACAGTTTAATGGGCACGTCCAC			n/a	1:200	Cryosections
zf-zic2a fwd	ACAACAATCTGTCGCCTTCCTC			n/a	1:200	whole-mount
zf-zic2a rev	ACAAATGCCCCTGTTTAGCCC			n/a	1:200	whole-mount
zf-zic2b fwd	TCTTCCGCTACATGCGACAAC			n/a	1:200	whole-mount
zf-zic2b rev	GCAACACCGACATGCTGAGAAC			n/a	1:200	whole-mount
zf-ephb1 fwd	CGCGTGTGGATGGATTACGG			n/a	1:200	whole-mount
zf-ephb1 rev	CATCCCCACCAGCTGGATCA			n/a	1:200	whole-mount
zf-atoh7 fwd	GGAGAAGTTTGAGAGTGCTATGCGG			n/a	1:200	whole-mount
zf-atoh7 rev	CGACTTTGAGCTGAGCACACACC			n/a	1:200	whole-mount
zf-rx2 fwd	GATACCATGAACATGGTGGACGATGG			n/a	1:200	whole-mount
zf-rx2 fwd	CCATCGACTGAATGTGCTCCTTGG			n/a	1:200	whole-mount
Primary antibodies						
Antigen	**Species**	**Catalog #**	**Company**	**RRID**	**Dilution**	**Immunohistochemistry**
Islet1	Rabbit	GTX128201	GeneTex	Ab_2868422	1:300	Cryosections/whole-mount
Acetylated-tubulin	Mouse	T6793	Sigma	Ab_477585	1:300	Cryosections/whole-mount
PCNA	Mouse	P8825	Sigma	Ab_477413	1:500	Cryosections
Islet1+2	Mouse	39.4D5	DSHB	Ab_2314683	1:50	Cryosections
GFP	Chicken	GTX13970	GeneTex	Ab_371416	1:5000	whole-mount
Rbpms	Guinea Pig	ABN1376	Millipore	Ab_2687403	1:400	Cryosections/flat-mount/ whole-
Zic2	Rabbit	Ab150404	Abcam	Ab_2868423	1:300	Cryosections/flat-mount/ whole-
Sox2	Goat	Sc17320	Santa-Cruz	Ab_2286684	1:300	flat-mount
EphB1	Mouse	MAb EfB1-3	DSBH	Ab_2314357	1:5	Cryosection
Secondary antibodies						
Anti-Rabbit cy3	Donkey	711-165-152	Jackson ImmunoResearch	Ab_2307443	1:500	cryosections/whole-mount
Anti-Rabbit Alexa Fluor 647	Donkey	711-605-152	Jackson ImmunoResearch	Ab_2492288	1:500	cryosections/Flat-mount/whole-mount
Anti-Goat Alexa Fluor 488	Donkey	A11055	Life Technologies	Ab_2534102	1:500	cryosections/Flat-mount/whole-mount
Anti-Goat Alexa Fluor 555	Donkey	A21432	Life Technologies	Ab_2535853	1:500	cryosections/Flat-mount/whole-mount
Anti-Goat Alexa Fluor 647	Bovine	805-605-180	Jackson ImmunoResearch	AB_2340885	1:600	cryosections
Anti-Goat cy3	Donkey	705-165-147	Jackson ImmunoResearch	Ab_2307351	1:500	cryosections/Flat-mount/whole-mount
Anti-mouse Alexa Fluor 488	Donkey	A21202	Life Technologies	Ab_141607	1:500	cryosections/Flat-mount/whole-mount
Anti-Guinea-Pig Alexa cy3	Donkey	706-165-148	Jackson ImmunoResearch	Ab_2340460	1:500	cryosections/Flat-mount/whole-mount
Anti-mouse Alexa Fluor 647	Donkey	715-605-150	Jackson ImmunoResearch	Ab_2340862	1:500	cryosections/Flat-mount/whole-mount
Anti-Mouse, Alexa Fluor 635	Goat	A31574	Life Technologies	Ab_2536184	1:500	cryosections
Anti-Rabbit, Alexa Fluor 568	Goat	A11036	Life Technologies	Ab_10563566	1:500	cryosections
Anti-Mouse, Alexa Fluor 568	Goat	A11004	Life Technologies	Ab_2534072	1:500	cryosections
Alexa Fluor 488 anti-chicken	Goat	A11039	Life Technologies	Ab_142924	1:500	cryosections
Tracers						
Cholera toxin subunit B-AlexaFluor555	n/a	C22843	Life technologies	n/a	2 µg/µl	Whole-mount
Cholera toxin subunit B-AlexaFluor647	n/a	C34778	Life technologies	n/a	2 µg/µl	Whole-mount

Movie S1.

Visual projections in teleosts.

Whole brain rendering of visual projections in 5 teleosts, the zebrafish, Mexican tetra, green-spotted pufferfish, mudskipper and butterflyfish. All species shows a complete decussation of retinal projections except the butterflyfish. All fish had bilateral eye injections of CTb coupled to either an Alexa Fluor-555 or and Alexa Fluor-647.

Movie S2.

Bilateral visual projections in non teleosts.

Whole brain rendering of visual projections in spotted gar, sterlet and armored bichir. Ipsilateral projections are seen in all species observed. All fish had bilateral eye injections of CTb coupled to either an Alexa Fluor-555 or and Alexa Fluor-647.

Movie S3.

The Australian lungfish possesses non-segregated ipsilateral projections.

Whole brain rendering of visual projections in the Australian lungfish, a sarcopterygian, injected with either an Alexa Fluor-555 or an Alexa Fluor-647. Many ipsilateral projections are observed, with a major component in the optic tectum. Ipsilateral projections are intermingled with contralateral projections in the optic tectum.

Movie S4.

ZIC2 expression is evolutionarily conserved in Humans.

Whole-mount immunohistochemistry of pcw9 human eyes using EyeDISCO clearing and labeled for the ipsilateral transcription factor ZIC2 (magenta) and the pan-retinal ganglion cell marker RBPMS (green). A large ZIC2-positive region can be seen in the temporal retina.

Movie S5.

Development of the *Lepisosteus oculatus* visual system.

3D rendering of 2-3 dpf, 6-7 dpf, and 17-18 dpf spotted gar embryos using EyeDISCO clearing and light-sheet fluorescence microscopy. Spotted gar embryos were labeled with the pan-neuronal marker acetylated tubulin (a-tubulin, green) and the LIM/homeodomain family of transcription factor Islet1, which is critical for the proper specification of retinal ganglion cells and motor neurons (magenta).

Supplementary Materials for

Bilateral visual projections exist in non-teleost bony fish and predate the emergence of tetrapods

Robin J. Vigouroux, Karine Duroure, Juliette Vougny, Shahad Albadri, Peter Kozulin, Eloisa Herrera, Kim Nguyen-Ba-Charvet, Ingo Braasch, Rodrigo Suarez, Filippo Del Bene* and Alain Chédotal*

Correspondence to: filippo.del-bene@inserm.fr and alain.chedotal@inserm.fr

This PDF file includes:

Materials and Methods
Figs. S1 to S7
Table S1
Captions for Movies S1 to S5

Other Supplementary Materials for this manuscript include the following:

Movies S1 to S5

Material and Methods

Animals

Juvenile Mexican tetra (San Solomon Spring, Balmorhea State Park, Texas, USA) were maintained at 26°C (surface fish) on a 12:12 h light:dark cycle. Juvenile zebrafish and embryos were maintained at 28.5°C on a 14 h light/10 h dark cycle. Juvenile Australian lungfish (10.2-13.5 cm body length; Jardini Pty Ltd, Brisbane, Australia) were on freshwater at 26°C on a 12:12 h light:dark cycle. Juvenile armored bichir, sterlet sturgeon, African butterflyfish, redeye piranha, atlantic mudskipper, green puffer fish and four-eyed fish, were acquired from commercial vendors. Spotted gar embryos were spawned at Nicholls State University in Louisiana and then raised and maintained at Michigan State University as previously described (*65*). Embryos were raised at 18°C which leads to a comparatively slow progression through the Long & Ballard stages of gar development (*48*). Sizes of each specimen were recorded for future analysis. Juvenile specimens of either sex were used. All animal procedures were performed under the in accordance with protocols approved by Sorbonne Université and Institut Curie (EU0143-21323 and APAFIS #6031-2016070822342309), Queensland Brain Institute (#QBI/041/20/France) and Michigan State University (#10/16-179-00).

Human eye samples

Human fetal eyes from terminated pregnancies were obtained from the INSERM-funded Human Developmental Cell Atlas collection (HuDeCA, https://hudeca.genouest.org/). All tissues were collected with appropriate maternal consent and approval from the French National Biomedicine agency (N° PFS19-012).

In Situ Hybridization

Spotted gar sections were hybridized with digoxigenin-labeled riboprobes as described in (*66*). Briefly, tissue sections were postfixed for 10 min in 4% paraformaldehyde (PFA) before being treated with Proteinase K (10 µg/ml; Invitrogen, #03115852001) for 2 min and subsequently postfixed for 5 min in 4% PFA. Sections were then acetylated and permeabilized in PBS, 1% Triton X-100. Sections were first homogenized with hybridization buffer (50% formamide (VWR #24311.291), 5× SSC (Euromedex, #EU0300-A), 1× Denhardt's, 250 µg/ml yeast tRNA, and 500 µg/ml herring sperm DNA, pH 7.4) for 2 h at RT and then hybridized overnight at 72°C with riboprobes (1/200), see Table S1 for probe sequences. The next day, sections were rinsed for 2 h in 2× SSC at 72°C, and blocked in 0.1 M Tris, pH 7.5, 0.15 M NaCl (B1) containing 10% normal goat serum (NGS) for 1 h at RT. After blocking, slides were incubated o/n at 4°C with anti-DIG antibody conjugated with the alkaline phosphatase (1/5000, Roche Diagnostics) or anti-DIG antibody conjugated with peroxidase in B1 containing 1% NGS. After washing in B1 buffer, the alkaline phosphatase activity was detected by using nitroblue tetrazolium chloride (337.5 µg/ml) and 5-bromo-4-chloro-3-indolyl phosphate (175 µg/ml) (Roche Diagnostics). The peroxidase activity was detected by using Tyramide Signal Amplification (TSA) (PerkinElmer, #NEL741001KT) and incubated with Fluorescein fluorophore Tyramide diluted at 1:50 in TSA. Sections were mounted in Mowiol (Calbiochem/Merck, Carlstadt, Germany).

Whole-mount in situ hybridization were carried out on zebrafish as previously described (*67*). Embryos were then embedded in gelatin/albumin with 4% of glutaraldehyde and sectioned (20 μm) on a VT1000 S vibrating blade microtome (Leica). Slides were scanned with either a Nanozoomer (Hamamatsu) or laser scanning confocal microscope (Olympus, FV1000).

Fluorescent in Situ Hybridization

To generate anti-sense probes, DNA fragments were obtained by PCR using Phusion™ High-Fidelity DNA polymerase (Thermo Scientific, #F530L) with the primers listed in Table S1. Total cDNA from 1 to 5 dpf zebrafish were used as a template. PCR fragments were cloned into the pCRII-TOPO vector (Invitrogen, #K280040) according to manufacturer's instructions. All plasmids used were sequenced for confirmation. Anti-sense DIG or fluorescein-labeled riboprobes were *in vitro* transcribed using the RNA labeling kit (Roche, #11685619910 or #11277073910) according to manufacturer's instructions. De-chorionated embryos at the appropriate developmental stages were fixed in fresh 4% PFA in 1X PBS (pH7.4) containing 0.1% Tween20 (PBSTw) for 4 h at RT and stored o/n in 100% methanol. Embryos were re-hydrated by immersing them in subsequent baths of 50% methanol/PBSTw (Sigma, #34860) and then twice in PBSTw, baths followed by a 10 min incubation in a 3% H_2O_2/0.5%KOH (Sigma, #P5958) solution. Embryos were then rinsed in 50% methanol and post-fixed in 100% methanol at -20°C for 2 h. Embryos were then re-hydrated in methanol/PBSTw (75%/50%/25%) followed by treatment in 10 µg/ml proteinase K at RT (1 dpf = 5 min, 2 dpf = 15 min, 3 dpf = 20 min), and post-fixed for 20 min in 4% PFA in PBSTw. Embryos were pre-hybridized at 68°C, and hybridized with either a fluorescein-labelled probe or DIG-labelled probe or both probes for dFISH assays o/n at 68°C with gentle shaking. Embryos were then rinsed at 68°C in 50% formamide/2XSSC/0.1%Tween-20 twice, 2XSSC/0.1%Tween-20, 0.2XSSC/0.1% Tween-20 twice and finally in TNT buffer (0.1 M Tris pH7.5, 0.15 M NaCl, 0.1% Tween-20). Blocking was done in TNB buffer (2% DIG block (Roche, #11096176001) in TNT) for 2 h at RT and incubated o/n with anti-Fluo-Fab-POD (Roche, #11426346910) diluted at 1:50 in TNB buffer at 4°C. All steps were performed in the dark. Embryos were then washed several times in TNT, rinsed using 100 μl Tyramide Signal Amplification (TSA) (PerkinElmer, #NEL741001KT) and incubated with Fluorescein fluorophore Tyramide diluted at 1:50 in TSA.

The reaction was stopped by 5 rapid washes of TNT. For dFISH assays, the DIG-labelled probe was then revealed by carrying out a 20 min incubation in 1%H_2O_2/TNT (Sigma, #18312-1L), then washed several times in TNT. A second blocking step was carried out for 1 h in TNB buffer prior to incubating embryos in anti-DIG-POD (Roche, #11207733910) diluted at 1:100 in TNB buffer o/n at 4°C. Revelation was done with Cy3 Fluorophore Tyramide solution (PerkinElmer, NEL#744001KT), washed with TNT and processed for imaging upon DAPI staining.

Molecular cloning

14xUAS:ubc-ZIC2-T2A-GFP-pA or *14xUAS:ubc-T2A-GFP-pA* were obtained via Gibson assembly using the *pT1UciMP Tol1* (Addgene, #62215) destination vector described by (*68*). *Tol1*mRNA was synthesized from the plasmid (Addgene, #61388) digested by NotI (NEB, #R3189S) and retro-transcribed with SP6 RNA polymerase (Roche, #10810274001). Human ZIC2 (*hZIC2*), *GFP*, and *T2A* were amplified via PCR from pCAG-hZIC2 and *pUAS:Cas9T2AGFP;U6:sgRNA1;U6sgRNA2* (Addgene, #74009) respectively using the NEBuilder HiFi DNA Assembly Cloning kit (NEB, #E5520). Appropriate sequences were inserted after the *UBC* intron of the *pT1UciMP Tol1* destination vector opened by restriction digest with NcoI-HF (NEB).

Alignment between the amino acid sequences of the Zic2 proteins zing finger domains

A multiple sequence alignment was performed for the region covering the ZIC2 zinc finger domains of NCBI Reference Sequence proteins of mouse (NP_033600), human (NP_009060) and zebrafish (ZIC2a NP_571633, ZIC2b NP_001001820), as well as for genome-predicted ZIC2 proteins the spotted gar (XP_006638968). The UniProtKB/Swiss-Prot curated zinc finger sequences of human ZIC2 (O95409) were used to delineate the domain positions within the alignment. Protein sequence alignment was performed using MUSCLE version 3.8.31 (*69*), the amino acid conservation at each aligned position visualised using BIS2Analyzer (*70*).

Eye enucleation

The transgenic line *Tg*(*atoh7:gal4-vp16*) (RRID: ZFIN_ZDB-GENO-130306-1) was used. Prior to eye enucleation, fish were selected for the atoh7 expression in green. At 2 dpf, eye enucleation was performed. The embryos were anesthetized in 0.004% tricaine MS222 in a 2% agarose gel solution (Life technologies, #16520050). One eye was surgically removed using a pulled capillary and mouth pipetting. Embryos were then transferred into fish medium (egg medium with penicillin/streptomycin (Life Technologies, #15140122) and 0.003% 1-phenyl-2-thiouera (Sigma, #189235) until 5 dpf, for whole-mount immunohistochemistry.

Immunohistochemistry

Cryosections

Spotted gar embryos were fixed by immersion in 4% PFA in 0.12 M phosphate buffer (VWR, 28028.298 and 28015.294), pH 7.4 (PFA) o/n at 4°C. Following three washes in 1XPBS, the samples were incubated in 10% sucrose (VWR, 27478.296) in 0.12 M phosphate buffer o/n at 4°C. The next day, samples were transferred to a 30% sucrose solution in 0.12 M phosphate buffer o/n at 4°C. Samples were then embedded in 0.12 M phosphate containing 7.5% gelatin (Sigma, 62500) and 10% sucrose, frozen in isopentane at -40°C and then cut at 16 μm with a cryostat (Leica, CM3050S). Sections were blocked in PBS containing 0.2% gelatin (VWR) and 0.25% Triton-X100 (PBS-GT) for 1 h at RT. Following the blocking, sections were incubated with primary antibodies (see Table S1) diluted in a PBS-GT solution o/n at RT. Following three washes in PBST (0.05% Trinton-X100) secondary antibodies coupled to the appropriate fluorophore (see Table S1) were diluted in PBS-GT and incubated for 2 h at RT. Sections were counterstained with Hoechst (Sigma, B2883, 1:1000) or DAPI (Life Technologies, D3571, 1/500). For PCNA staining, an antigen retrieval step was performed by boiling sections in a 1X Sodium Citrate solution pH 6.0 for 5 min using a microwave. This step was skipped when the samples were first used for an *in-situ* hybridization assay. Slides were scanned with either a Nanozoomer (Hamamatsu) or laser scanning confocal microscope (Olympus, FV1000).

Whole-mount Immunohistochemistry

Zebrafish whole-mount immunohistochemistry was adapted from (*61*). Briefly, embryos were fixed in 4% PFA diluted in PBS containing 0.1% Tween-20 (VWR, #0777-1L) (PBSTw) for 4 h at RT and stored o/n in 100% methanol. After re-hydration, embryos were incubated for 20 min at -20°C in already pre-chilled acetone (Sigma, #650501). The embryos were rinsed several times with PBSTw and blocked for 2 h in blocking solution (10% bovine serum albumin (BSA) (Euromedex, #04-100-812-C), 10% normal goat serum (LifeTechnologies, #1000C), 1% DMSO (Sigma Aldrich, #D8418) in PBSTw). The primary antibodies were incubated o/n at 4°C in 1% BSA, 1% normal goat serum, 0.1% DMSO in PBSTw according to the dilutions in Table S1. After several washes in PBSTw, the secondary antibodies were incubated o/n at 4°C. The next day, embryos were rinsed in PBSTw and processed for imaging.

Whole-mount immunostaining on spotted gar embryos was carried out as previously described (*15*). Briefly, embryos were depigmented in a solution of 11% H_2O_2 (VWR, 216763) at 70 rpm exposed to an 11W warm white Light-Emitting Diode (LED) (3000° Kelvin) for 1-3 days. Samples were then blocked and permeabilized before being incubated with the primary antibodies for 7 days at RT (see Table S1) in a solution containing: 0.5% Tirton-X100, 5% donkey normal serum, 20% Dimethyl Sulfoxide, 1XPBS, 0.1 g/L thimerosal. The samples were further labeled with secondary antibodies (see Table S1) for 2 days at RT under agitation.

Retinal flat-mounts

For retinal flat mounts, human eyes were harvested and fixed in 4% PFA, followed by three washes in 1XPBS. Eyes were then de-pigmented using the EyeDISCO protocol as previously described (*15*). For immunohistochemistry, retinas were permeabilized and blocked in a solution containing 0.5% Triton-X100, 5% donkey normal serum, 1XPBS, 0.1 g/L thimerosal for 1 day at RT under agitation. Primary antibodies (see Table S1) were diluted in a solution containing 0.5% Triton-X100, 5% donkey normal serum, 20% Dimethyl Sulfoxide, 1XPBS, 0.1 g/L thimerosal for 3 days at RT under agitation. The retinas were then washed for 1 day in PBST (1XPBS, 0.5% Triton-X100). The secondary antibodies (see Table S1) were diluted in the same solution as primary antibodies and left for 2 days. After washing retinas for 1 day, they were mounted on slides and imaged using a scanning confocal microscope (Olympus, FV1000).

Tracing of visual projections

All fish were anesthetized with 0,04% MS222, tricaine-methanesulfonate (Sigma, #E10521) diluted in fish water. Australian lungfish were anesthetized with 0.05% clove oil in fresh water. Injection of cholera toxin β subunit was carried out as described in (*15*). Briefly, using a capillary approximately 1µl of 2 µg/µl of Alexa Fluor-conjugated cholera toxin β subunit (Thermo Fischer, Alexa Fluor555-CTb C22843 and Alexa Fluor647-CTb C34778) was injected intravitreally. 72-96 h following CTb injection, specimens were transcardially perfused with 4%PFA and the heads and/or brains were dissected for tissue clearing.

Tissue clearing and imaging

Clearing

Prior to clearing, spotted gar *embryos* were embedded in 1.5% agarose (Roth) in 1X TAE (Life Technologies). Clearing was carried out as previously described (*15*). Briefly, samples were gently de-hydrated in ascending baths of methanol (1.5 h). Samples were further treated with a solution containing 2/3 Dichloromethane (DCM, Sigma) 1/3 methanol o/n. The next day, samples were placed in DCM for 30 min prior to being immersed in Di-benzyl Ether (DBE, Sigma).

Imaging

Acquisitions were performed by using an UltraMicroscope I (Miltenyi Biotec, Germany) or UltraMicroscope Blaze (Miltenyi Biotec, Germany) with the ImspectorPro software (Miltenyi Biotec, Germany, 5.1.328 version). The light sheet was generated by a laser (wavelength 488, 561, 647 Coherent Sapphire Laser, LaVision BioTec, Miltenyi Biotec, Germany) or a second-generation laser beam combiner (wavelengths 488 nm, 561 nm and 647 nm; LaVision BioTec, Miltenyi Biotec, Germany). All light sheets were matched within their Rayleigh lengths for optimal illumination at the sample site. Either a binocular stereomicroscope (Olympus, MXV10) with a 2x objective (Olympus, MVPLAPO) was used Or a MI Plan 1.1x (NA = 0.1), a MI Plan 4x (NA = 0.35), and a MI Plan 12x (NA = 0.53) objectives were used (Miltenyi Biotec, Germany). Samples were placed in an imaging reservoir made of 100% quartz (LaVision BioTec, Miltenyi Biotec) filled with DBE and illuminated from the side by the laser light. A Zyla sCMOS camera (Andor, Oxford Instrument; 2,048 × 2,048, 6.5 x 6.5 μm^2, peak QE 82%) was used to acquire images. The step size between each image was fixed at 1 or 2 µm (NA = 0.5, 150 ms time exposure). All tiff images are generated in 16-bit.

Confocal microscopy

Whole-mount 5 dpf zebrafish larvae were mounted in a labtex plates (LabTex) in 2.5% agarose or in 1% low-melting agarose on FluoroDish Cell Culture dish (FD3510-100, World Precision Instruments). For imaging, a scanning inverted confocal microscope (FV1200, Olympus) was used with a 30x objective (Olympus, UPLSAPO30XS, NA = 1.05, WD = 0.8 mm) as well as the LSM780 and LSM880 scanning inverted confocal microscopes (Zeiss) for high resolution microscopy. 40x water immersion objective for whole mount dFISH stained zebrafish embryos and 63x oil objective for zebrafish retinal cryosections were used and a 10x air objective was used to image the spotted gar cryosections.

Image Processing

3D rendering of light sheet and confocal stacks were converted to an Imaris file (.ims) using ImarisFileConverter (Bitplane, 9.5.1 version) and then visualized using the Imaris x64 software (Bitplane, 9.5.1). To quantify ipsilateral territories, entire tectum volume and ipsilateral projections were automatically segmented with a surface detail of 5.00 μm, automatic threshold. Volumes were extracted from the surface. Movies were generated using the animation tool on Imaris x64 software (Bitplane, version 9.1.2) and movie reconstruction with .tiff series were done using ImageJ (1.50e, Java 1.8.0_60, 64-bit). All movie editing (text and transitions) was performed using iMovie (Apple Inc., version 10.1.1).

To quantify the ipsilateral projections in the hZIC2 overexpression experiments, a fixed region of interest was identified for each zebrafish (corresponding to the ipsilateral and contralateral optic tecta). Retinal projections were segmented with a surface detail of 0.5 μm using an automatic threshold. Ipsilateral and contralateral volumes were extracted and summed to constitute the "total visual projections" using Imaris x64 software (Bitplane, version 9.1.2). The volume of ipsilateral projections was isolated as a ratio of ipsilateral projections:total projections.

Statistical analyses

All data are described are listed as biological replicates (n) and all experiments (N) were carried out at least in triplicates unless indicated otherwise). An observer blinded to the experimental conditions realized all the quantifications. No data were excluded from the statistical analyses. All data are represented as mean values ± SEM. Statistical significance was estimated using two-tailed unpaired tests for non-parametric tendencies (Kruskall-Wallis or Mann-Whitney), two-way ANOVA and Bonferroni's multiple comparison test. $* = p < 0.05$; $** = p < 0.01$; $*** = p < 0.001$, $*** = p < 0.0001$. All statistical measurements were carried out using GraphPad Prism 7.

Supplementary Figures

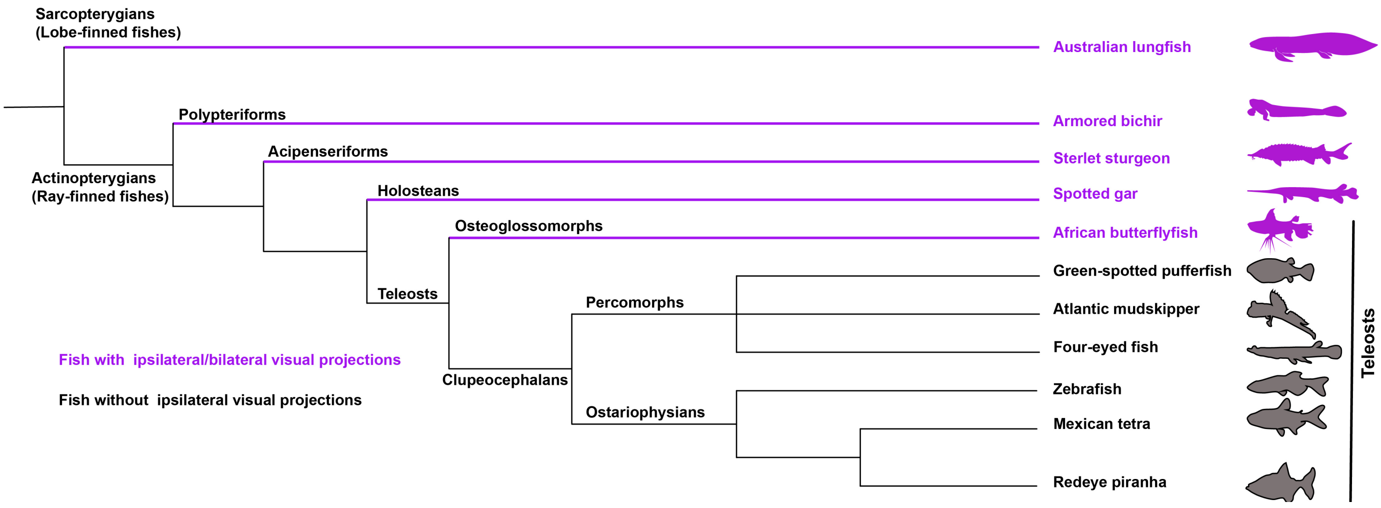

Fig. S1. Simplified chart of fish taxonomy indicating the species analyzed in this study.
Fish with bilateral/ipsilateral visual projections appear in magenta and fish with only contralateral visual projections appear in grey.

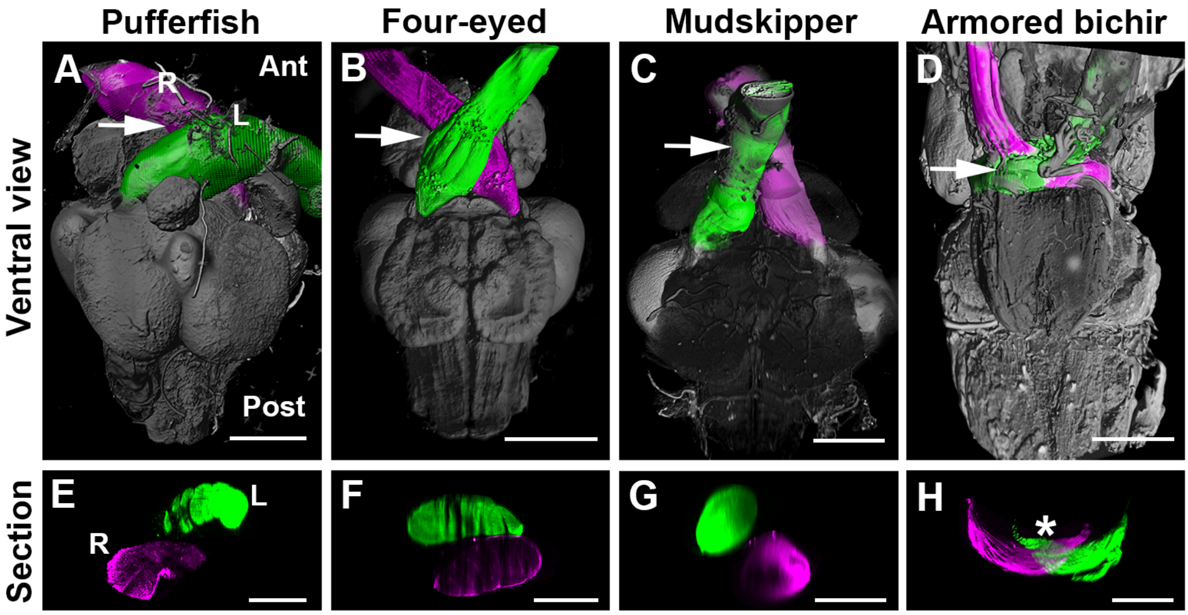

Fig. S2. Two types of optic nerve crossing modalities in ray-finned fishes.
Ventral views (**A** to **D**) and coronal optical sections (**E** to **H**) at the level of the optic chiasm of iDISCO-cleared brains and optic nerves. A surface rendering with normal shading (Imaris) was applied to generate the ventral view images. The arrowheads (A to D) indicate the level of the chiasm optical section in (E to H). In all fishes, one eye was injected with Alexa Fluor-555-conjugated CTb and the other one with Alexa Fluor-647-conjugated CTb. The right (R) and left (L) optic nerves were pseudo-colored in magenta and green respectively. In Pufferfish (A and E), Four-eyed (B and F) and Muskipper (C and G), the two optic nerves pass over and overlap at the chiasm but remain separated up to the brain. By contrast, in the Armored bichir (D and H), the right and left nerves meet at the chiasm and retinal ganglion cell axons from both eyes interweave during crossing (asterisk). Abbreviations: Ant, anterior; Post, Posterior. Scale bars are: 2 mm in (B), 1 mm in (A, C, D, F), 800 μm in (G), 600 μm in (E, H).

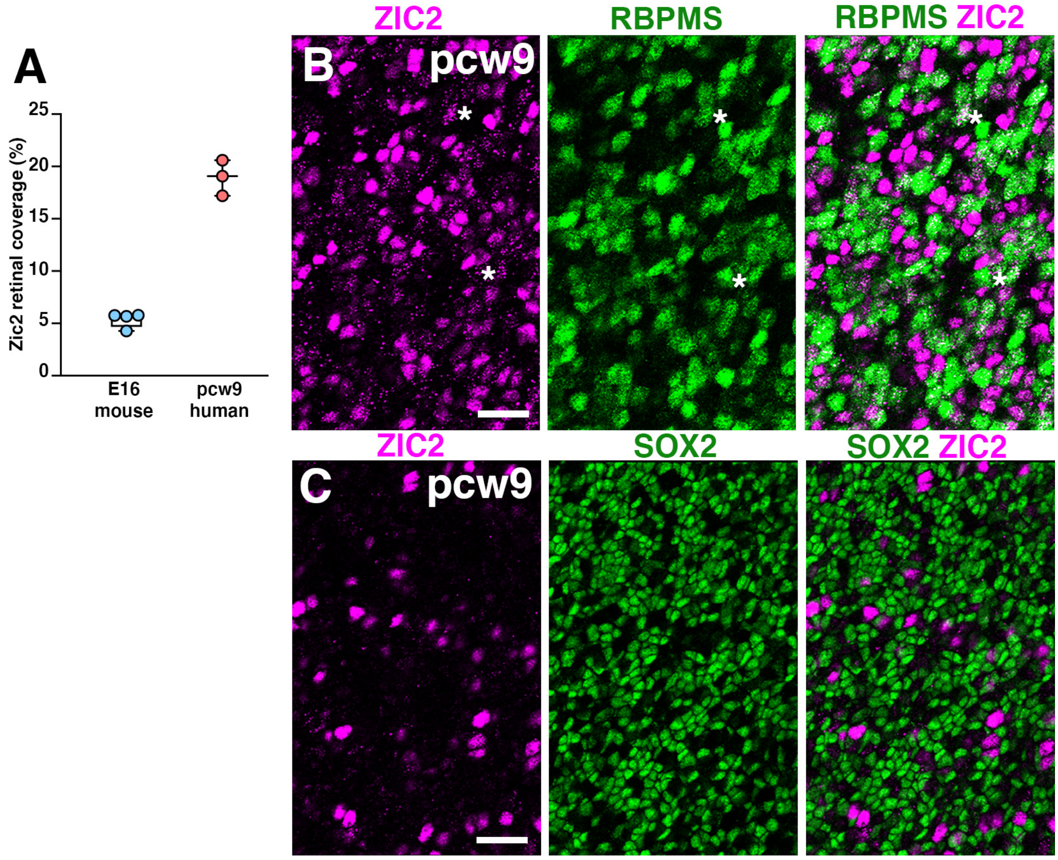

Fig. S3. ZIC2 expression pattern in human embryo retina.
(**A**) Box and whiskers representation of the ZIC2-positive surface in E16 mouse and pcw9 human retinas. (**B** and **C**) flat-mount pcw9 human retina labeled for ZIC2 and RBPMS (B) or SOX2 (C). (B) In the most superficial (basal side) regions of the temporal retina, ganglion cells expressing low levels of ZIC2 and RBPMS (arrowheads) are seen but ZIC2 and RBPMS are mostly exclusive. (C) image at the level of the interface between the neuroblastic layer showing that ZIC2+ cells are not SOX2+. Scale bars are: 50 μm in (B and C).

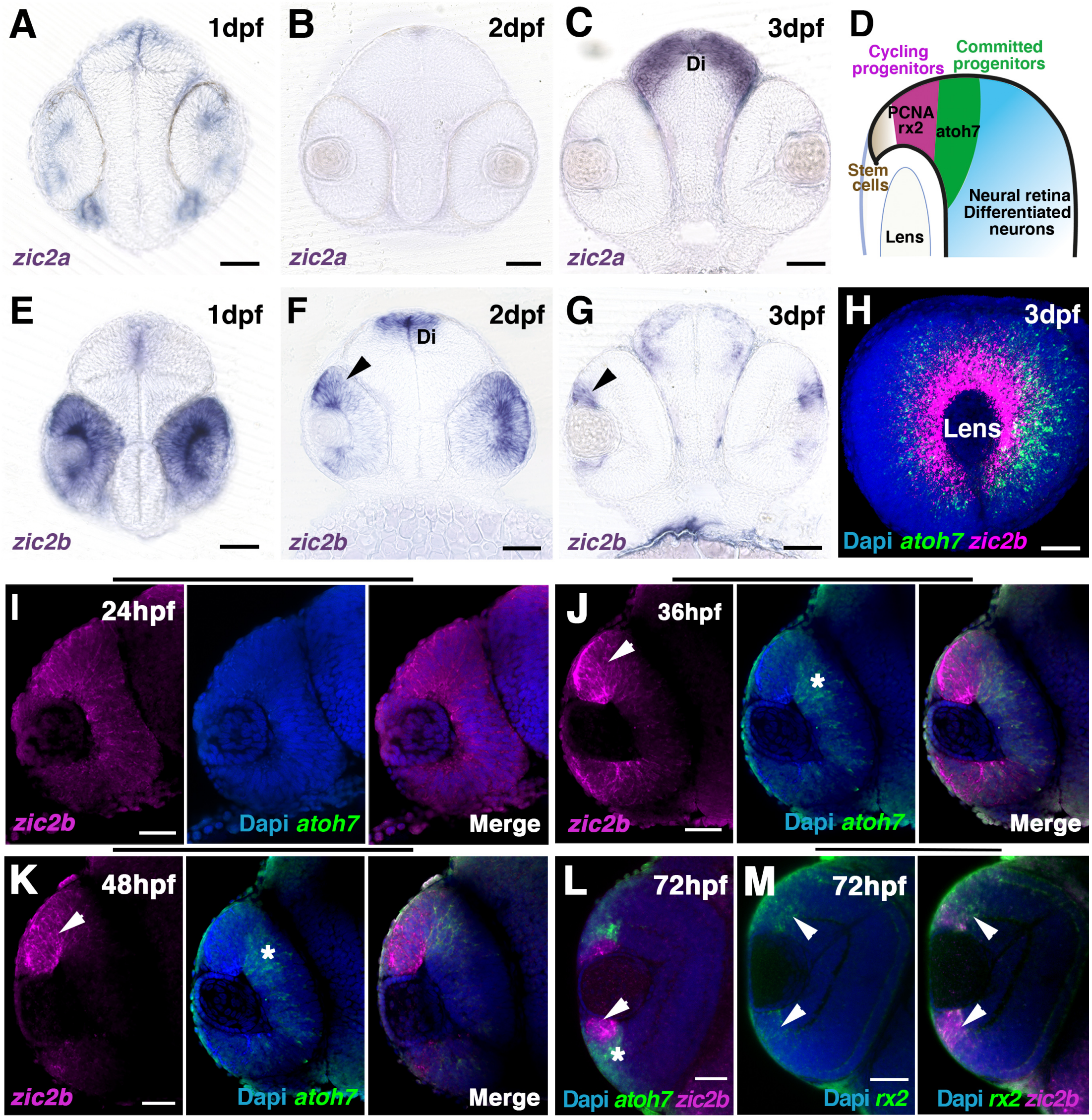

Fig. S4. Zic2 ortholog expression in zebrafish is restricted to the ciliary margin zone.
(**A** to **H**) Whole-mount *in situ* hybridization of zebrafish embryos for *zic2a* at 1 day post fertilization (1 dpf; A), 2 dpf (B) and 3 dpf (C) as well as *zic2b* at 1 dpf (E), 2 dpf (F) and 3 dpf (G). Zic2b is expressed in the ciliary marginal zone (CMZ, arrowheads in F and G) and in the dorsal diencephalon (Di). (D) Schematic drawing of the zebrafish CMZ in the developing retina showing spatial distribution of stem cells, cycling progenitors, committed progenitors and differentiated neurons. (H)**,** Lateral view of whole-mount double fluorescent *in situ* hybridization for *zic2b* and *atoh7* on 3 dpf zebrafish embryos with DAPI counterstaining. (I to L) Confocal sections through the central retina of wild-type embryos hybridized with antisense RNA probes for *zic2b* and *atoh7*. At 24 hpf, *zic2b* is expressed in the entire proliferative neuroepithelium and later from a central to peripheral wave-like manner (arrowheads) in complementarity to the neurogenic transient expression of *atoh7* (asterisks) as shown here for 36, 48 and 72 hpf. (L to M) Confocal sections through the central retina of 72 hpf wild-type zebrafish embryos hybridized with antisense RNA probes for *zic2b* and *retinal homeo- box transcription factor2* (*rx2*, a marker or dividing progenitors and stem cells in the CMZ). *Zic2b* expression overlaps with the expression of the *rx2* (arrowheads). All retinae were counterstained with the nuclear marker DAPI. Scale bars are 50 μm (A to C and E to H) and 40 μm (I to M).

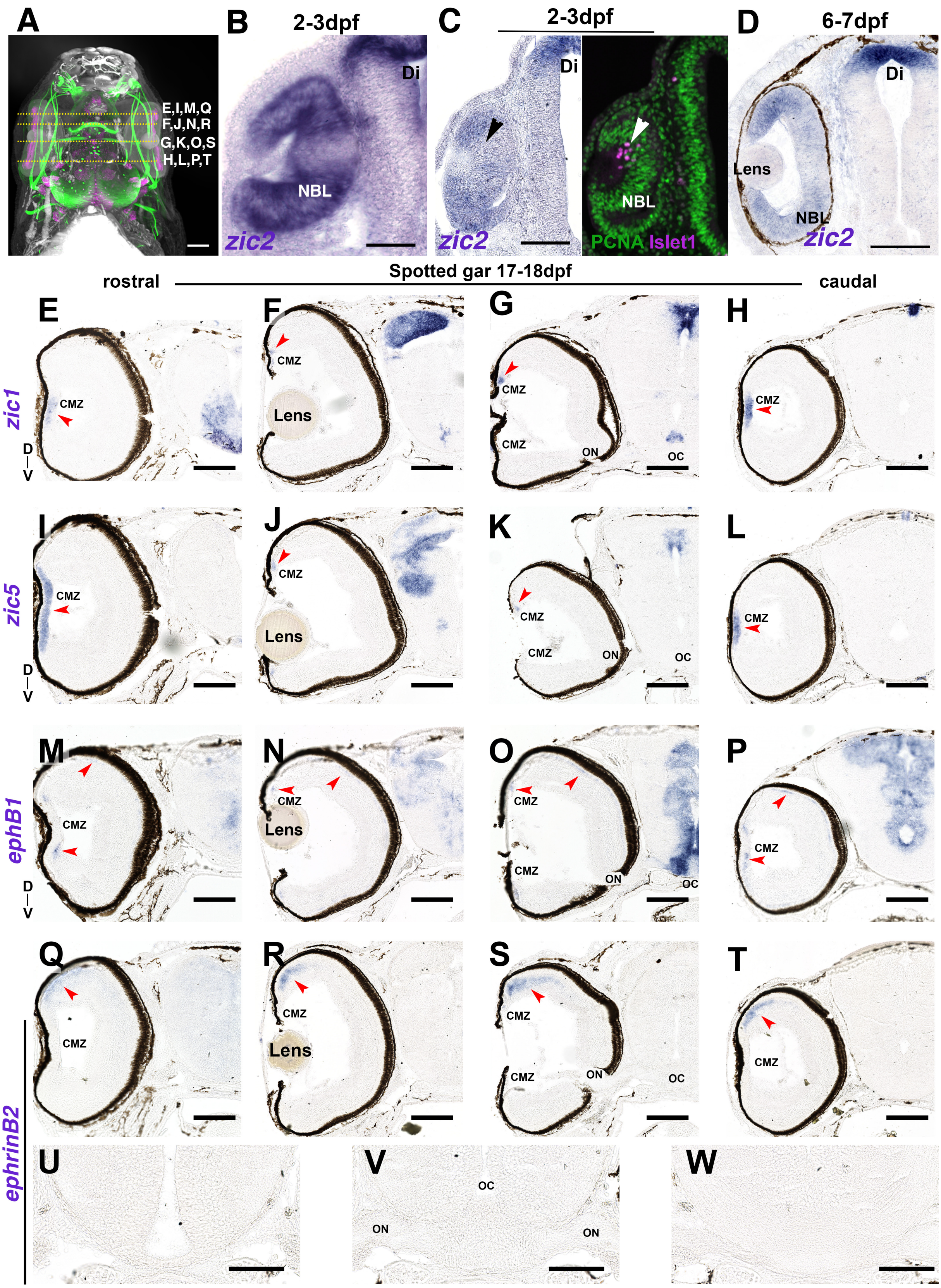
A
E,I,M,Q
F,J,N,R
G,K,O,S
H,L,P,T
B
2-3dpf
Di
NBL
zic2
C
2-3dpf
Di
zic2
NBL
PCNA Islet1
D
6-7dpf
Di
Lens
NBL
zic2
rostral
Spotted gar 17-18dpf
caudal
E
F
G
H
zic1
CMZ
Lens
ON
OC
D
V
I
J
K
L
zic5
M
N
O
P
ephB1
Q
R
S
T
ephrinB2
U
V
W

Fig. S5. Mammalian ipsilateral markers are not expressed in the spotted gar visual system.

(**A**) 3D light-sheet fluorescence microscopy images of iDISCO-cleared 17-18 dpf spotted gar indicating with dotted lines the anatomical levels of the cryosections. (**B** to **D**) *In situ* hybridization for *zic2* on retinal cryosections of the developing spotted gar at 2-3 dpf (B), 6-7 dpf (C, left panel), 17-18 dpf (D). Only proliferating cells in the neuroblastic layer (NBL) express *zic2*. The right panel in (C) is an immunostaining for PCNA and Islet1. The arrowheads in (C) indicate the region where the first ganglion cells (Islet1+) are present at this stage in the retina. *zic2* is also found in the diencephalon (Di). (**E** to **T**) Rostral-to-caudal coronal cryosections from 17-18 dpf spotted gar. *zic1* (E to H) and *zic5* (I to L) are only expressed in the ciliary marginal zone (CMZ; arrow). (**M** to **P**) *ephB1* is absent from the retina and weakly expressed in the CMZ. (**Q** to **T**) *ephrinB2* is expressed in the dorsal retina (arrow). (**U** to **W)** Cryosections of the diencephalon of a 17-18dpf spotted gar hybridized for *ephrinB2*. *ephrinB2* is absent from the optic chiasm (asterisk). Immuno-reactive regions are highlighted (arrowhead). Abbreviations: NBL, Neuroblastic layer; ON, Optic nerve, OC, Optic chiasm; GCL, Ganglion cell layer; INL, Inner nuclear layer; ONL, Outer nuclear layer. Scale bars: A, 200 μm; B to D, 50 μm; C,U to W, 100 μm; D to T, 250 μm.

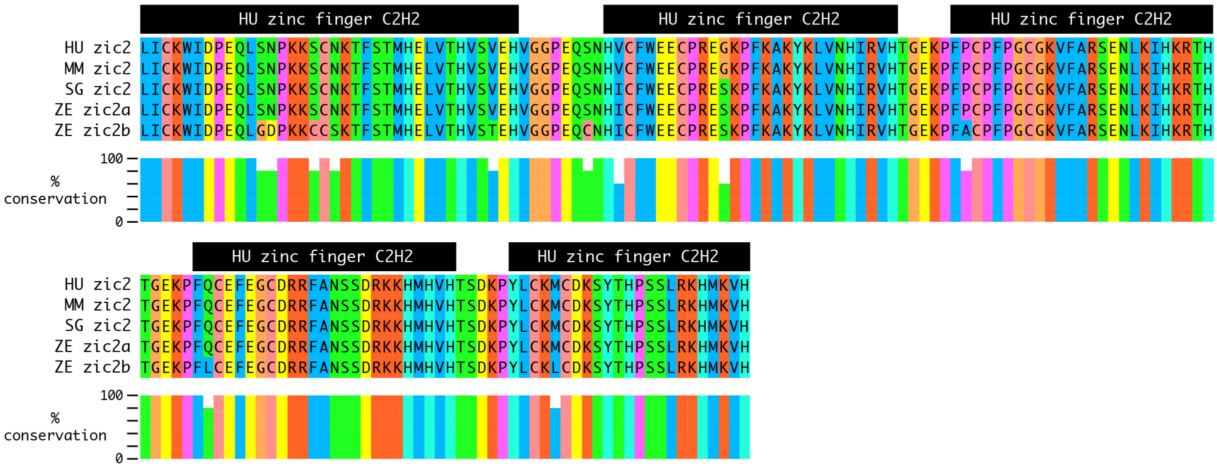

Fig. S6. Alignment between the amino acid sequences of the Zic2 protein zing finger domains of fish and mammals.

Alignment of Zic proteins across the zinc finger domains shows the high level of conservation between ray-finned fish and mammals. Amino acids are color coded according to the physiochemical class they belong to. Abbreviations: HU, human; MM, mouse; SG, spotted gar; ZE, zebrafish.

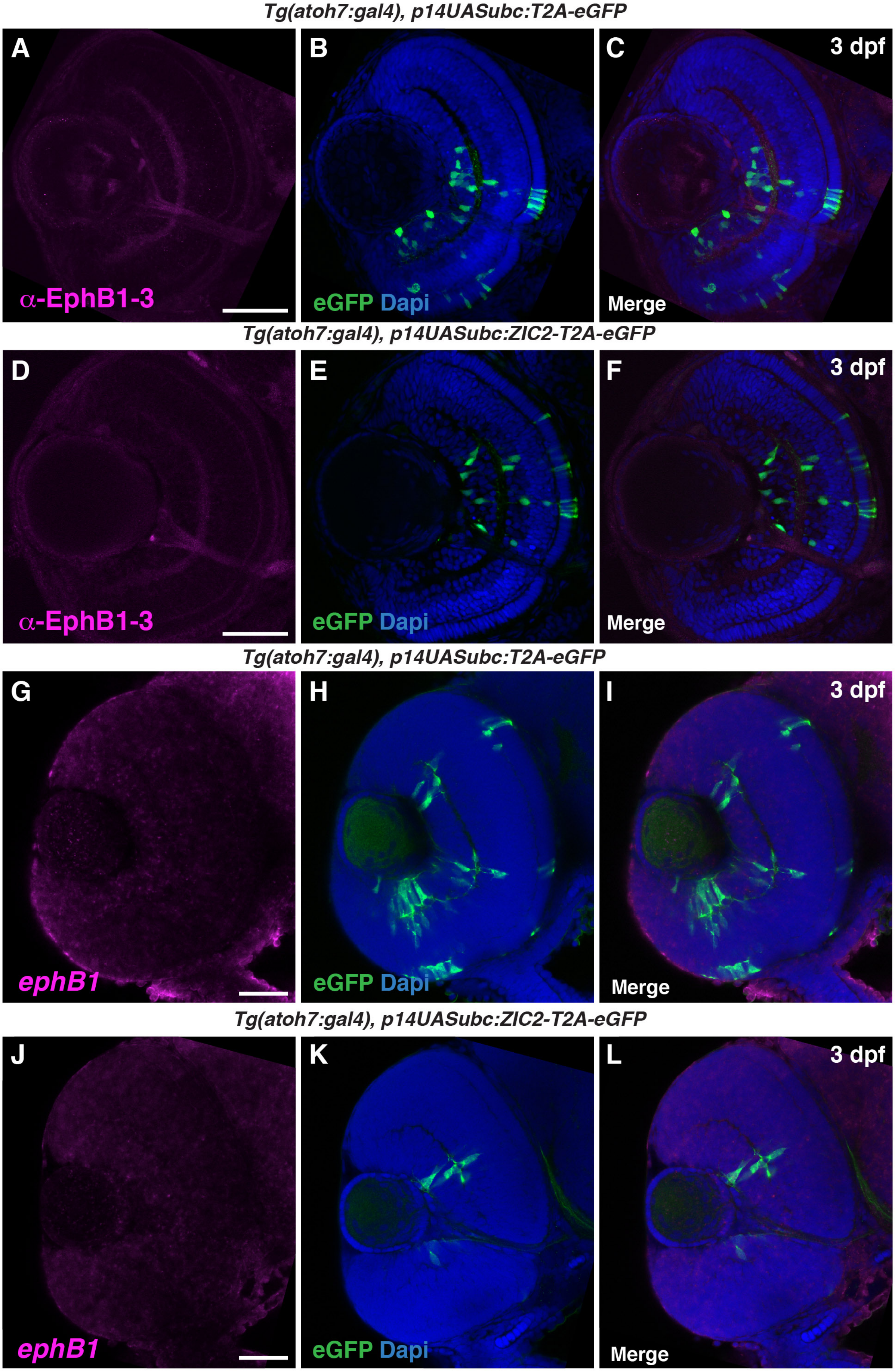
Tg(atoh7:gal4), p14UASubc:T2A-eGFP
A
B
C
3 dpf
α-EphB1-3
eGFP Dapi
Merge
Tg(atoh7:gal4), p14UASubc:ZIC2-T2A-eGFP
D
E
F
3 dpf
α-EphB1-3
eGFP Dapi
Merge
Tg(atoh7:gal4), p14UASubc:T2A-eGFP
G
H
I
3 dpf
ephB1
eGFP Dapi
Merge
Tg(atoh7:gal4), p14UASubc:ZIC2-T2A-eGFP
J
K
L
3 dpf
ephB1
eGFP Dapi
Merge

Fig.S7. Ectopic *ZIC2* expression in *atoh7* retinal progenitor cells does not induce EphB1 expression in retinal ganglion cells.

Confocal images of cryostat (**A-F**) or optical (**G-L**) sections of 3 dpf retinae from *Tg*(*atoh7:gal4*) embryos injected at 1-cell stage with either a *p14UASubc:T2A-eGFP* (A to C and G to I) control construct or a *p14UASubc:ZIC2-T2A-eGFP* construct (D to F and J to L). No signal for EphB1 in GFP-positive cells is detectable in all injected retinae either double stained with anti-EphB1 antibody (A to F) or hybridized with an *ephB1* antisense riboprobe (G to L). All retinae were counterstained with the nuclear marker DAPI. Scale bars are 50 μm.

Table S1. Comprehensive table summarizing the antibodies and probes sequences.

In situ probes						
Name	**Sequence**			**RRID**	**Dilution**	**In situ hybridization**
L-zic1 fwd	ACCTCCAGACATCACTCAAC			n/a	1:200	Cryosections
L-zic1 rev	GGAACACTCTTCCCAGAAAC			n/a	1:200	Cryosections
L-zic2 fwd	AAACTTAACCACGACCTCTCTC			n/a	1:200	Cryosections
L-zic2 rev	CTCGTGCATTGTGCTGAAAG			n/a	1:200	Cryosections
L-zic5 fwd	CTTTGAGCAAGAGGAATCCGGC			n/a	1:200	Cryosections
L-zic5 rev	CCTGCCGCGATGTTCACATTTA			n/a	1:200	Cryosections
L-efnb2 fwd	TCCCCATTATGAGAAGGTGAGCGG			n/a	1:200	Cryosections
L-efnb2 rev	ACAGGCTACCACTTCAGAAGGCAG			n/a	1:200	Cryosections
L-ephb1 fwd	AGAACCTGAACACAATCCGCAC			n/a	1:200	Cryosections
L-ephb1 rev	ACAGTTTAATGGGCACGTCCAC			n/a	1:200	Cryosections
zf-zic2a fwd	ACAACAATCTGTCGCCTTCCTC			n/a	1:200	whole-mount
zf-zic2a rev	ACAAATGCCCCTGTTTAGCCC			n/a	1:200	whole-mount
zf-zic2b fwd	TCTTCCGCTACATGCGACAAC			n/a	1:200	whole-mount
zf-zic2b rev	GCAACACCGACATGCTGAGAAC			n/a	1:200	whole-mount
zf-ephb1 fwd	CGCGTGTGGATGGATTACGG			n/a	1:200	whole-mount
zf-ephb1 rev	CATCCCCACCAGCTGGATCA			n/a	1:200	whole-mount
zf-atoh7 fwd	GGAGAAGTTTGAGAGTGCTATGCGG			n/a	1:200	whole-mount
zf-atoh7 rev	CGACTTTGAGCTGAGCACACACC			n/a	1:200	whole-mount
zf-rx2 fwd	GATACCATGAACATGGTGGACGATGG			n/a	1:200	whole-mount
zf-rx2 fwd	CCATCGACTGAATGTGCTCCTTGG			n/a	1:200	whole-mount
Primary antibodies						
Antigen	**Species**	**Catalog #**	**Company**	**RRID**	**Dilution**	**Immunohistochemistry**
Islet1	Rabbit	GTX128201	GeneTex	Ab_2868422	1:300	Cryosections/whole-mount
Acetylated-tubulin	Mouse	T6793	Sigma	Ab_477585	1:300	Cryosections/whole-mount
PCNA	Mouse	P8825	Sigma	Ab_477413	1:500	Cryosections
Islet1+2	Mouse	39.4D5	DSHB	Ab_2314683	1:50	Cryosections
GFP	Chicken	GTX13970	GeneTex	Ab_371416	1:5000	whole-mount
Rbpms	Guinea Pig	ABN1376	Millipore	Ab_2687403	1:400	Cryosections/flat-mount/ whole-
Zic2	Rabbit	Ab150404	Abcam	Ab_2868423	1:300	Cryosections/flat-mount/ whole-
Sox2	Goat	Sc17320	Santa-Cruz	Ab_2286684	1:300	flat-mount
EphB1	Mouse	MAb EfB1-3	DSBH	Ab_2314357	1:5	Cryosection
Secondary antibodies						
Anti-Rabbit cy3	Donkey	711-165-152	Jackson ImmunoResearch	Ab_2307443	1:500	cryosections/whole-mount
Anti-Rabbit Alexa Fluor 647	Donkey	711-605-152	Jackson ImmunoResearch	Ab_2492288	1:500	cryosections/Flat-mount/whole-mount
Anti-Goat Alexa Fluor 488	Donkey	A11055	Life Technologies	Ab_2534102	1:500	cryosections/Flat-mount/whole-mount
Anti-Goat Alexa Fluor 555	Donkey	A21432	Life Technologies	Ab_2535853	1:500	cryosections/Flat-mount/whole-mount
Anti-Goat Alexa Fluor 647	Bovine	805-605-180	Jackson ImmunoResearch	AB_2340885	1:600	cryosections
Anti-Goat cy3	Donkey	705-165-147	Jackson ImmunoResearch	Ab_2307351	1:500	cryosections/Flat-mount/whole-mount
Anti-mouse Alexa Fluor 488	Donkey	A21202	Life Technologies	Ab_141607	1:500	cryosections/Flat-mount/whole-mount
Anti-Guinea-Pig Alexa cy3	Donkey	706-165-148	Jackson ImmunoResearch	Ab_2340460	1:500	cryosections/Flat-mount/whole-mount
Anti-mouse Alexa Fluor 647	Donkey	715-605-150	Jackson ImmunoResearch	Ab_2340862	1:500	cryosections/Flat-mount/whole-mount
Anti-Mouse, Alexa Fluor 635	Goat	A31574	Life Technologies	Ab_2536184	1:500	cryosections
Anti-Rabbit, Alexa Fluor 568	Goat	A11036	Life Technologies	Ab_10563566	1:500	cryosections
Anti-Mouse, Alexa Fluor 568	Goat	A11004	Life Technologies	Ab_2534072	1:500	cryosections
Alexa Fluor 488 anti-chicken	Goat	A11039	Life Technologies	Ab_142924	1:500	cryosections
Tracers						
Cholera toxin subunit B-AlexaFluor555	n/a	C22843	Life technologies	n/a	2 μg/μl	Whole-mount
Cholera toxin subunit B-AlexaFluor647	n/a	C34778	Life technologies	n/a	2 μg/μl	Whole-mount

Movie S1.

Visual projections in teleosts.

Whole brain rendering of visual projections in 5 teleosts, the zebrafish, Mexican tetra, green-spotted pufferfish, mudskipper and butterflyfish. All species shows a complete decussation of retinal projections except the butterflyfish. All fish had bilateral eye injections of CTb coupled to either an Alexa Fluor-555 or and Alexa Fluor-647.

Movie S2.

Bilateral visual projections in non teleosts.

Whole brain rendering of visual projections in spotted gar, sterlet and armored bichir. Ipsilateral projections are seen in all species observed. All fish had bilateral eye injections of CTb coupled to either an Alexa Fluor-555 or and Alexa Fluor-647.

Movie S3.

The Australian lungfish possesses non-segregated ipsilateral projections.

Whole brain rendering of visual projections in the Australian lungfish, a sarcopterygian, injected with either an Alexa Fluor-555 or an Alexa Fluor-647. Many ipsilateral projections are observed, with a major component in the optic tectum. Ipsilateral projections are intermingled with contralateral projections in the optic tectum.

Movie S4.

ZIC2 expression is evolutionarily conserved in Humans.

Whole-mount immunohistochemistry of pcw9 human eyes using EyeDISCO clearing and labeled for the ipsilateral transcription factor ZIC2 (magenta) and the pan-retinal ganglion cell marker RBPMS (green). A large ZIC2-positive region can be seen in the temporal retina.

Movie S5.

Development of the *Lepisosteus oculatus* visual system.

3D rendering of 2-3 dpf, 6-7 dpf, and 17-18 dpf spotted gar embryos using EyeDISCO clearing and light-sheet fluorescence microscopy. Spotted gar embryos were labeled with the pan-neuronal marker acetylated tubulin (a-tubulin, green) and the LIM/homeodomain family of transcription factor Islet1, which is critical for the proper specification of retinal ganglion cells and motor neurons (magenta).

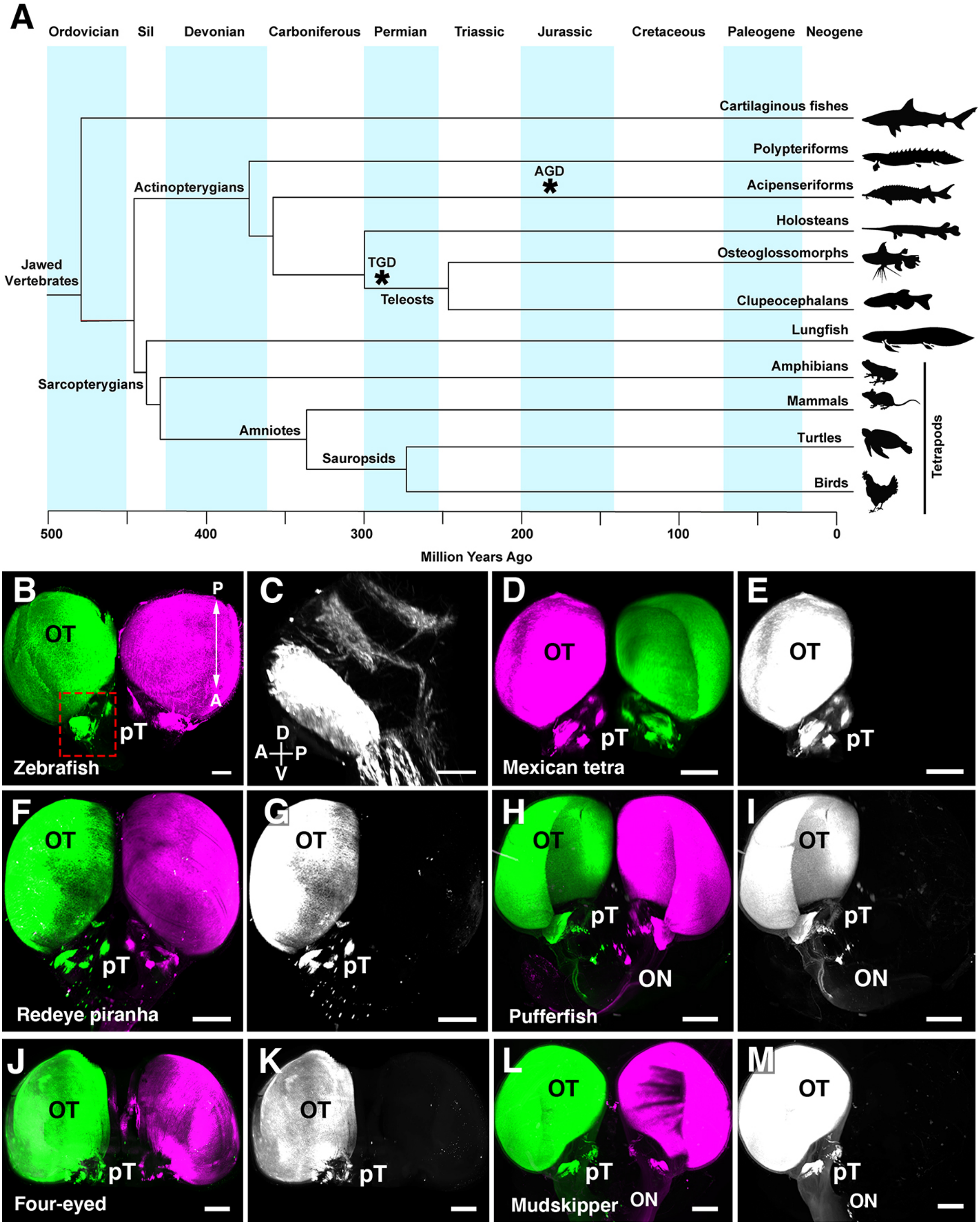
A
Ordovician
Sil
Devonian
Carboniferous
Permian
Triassic
Jurassic
Cretaceous
Paleogene
Neogene
Cartilaginous fishes
Polypteriforms
AGD
Actinopterygians
Acipenseriforms
Holosteans
Osteoglossomorphs
TGD
Jawed Vertebrates
Teleosts
Clupeocephalans
Lungfish
Amphibians
Sarcopterygians
Mammals
Amniotes
Turtles
Sauropsids
Birds
Tetrapods
500
400
300
200
100
0
Million Years Ago
B
OT
P
A
pT
Zebrafish
C
D
A
P
V
D
OT
pT
Mexican tetra
E
OT
pT
F
OT
pT
Redeye piranha
G
OT
pT
H
OT
pT
ON
Pufferfish
I
OT
pT
ON
J
OT
pT
Four-eyed
K
OT
pT
L
OT
pT
Mudskipper
ON
M
OT
pT
ON

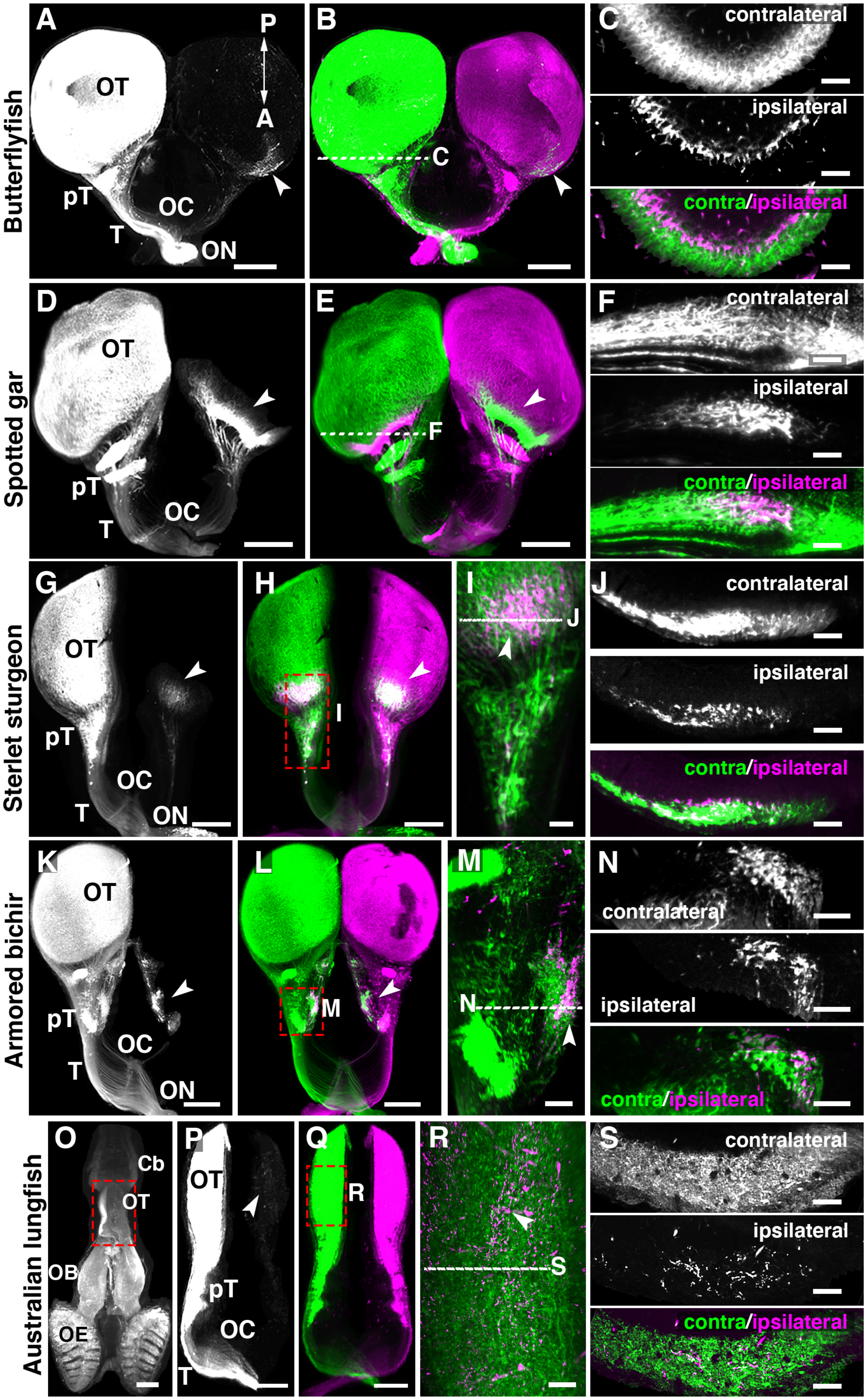

Butterflyfish
Spotted gar
Sterlet sturgeon
Armored bichir
Australian lungfish
A
P
A
OT
pT
T
OC
ON
B
C
contralateral
ipsilateral
contra/ipsilateral
D
OT
pT
T
OC
E
F
contralateral
ipsilateral
contra/ipsilateral
G
OT
pT
OC
T
ON
H
I
J
contralateral
ipsilateral
contra/ipsilateral
K
OT
pT
OC
T
ON
L
M
N
contralateral
ipsilateral
contra/ipsilateral
O
Cb
OT
OB
OE
P
OT
pT
OC
T
Q
R
S
contralateral
ipsilateral
contra/ipsilateral

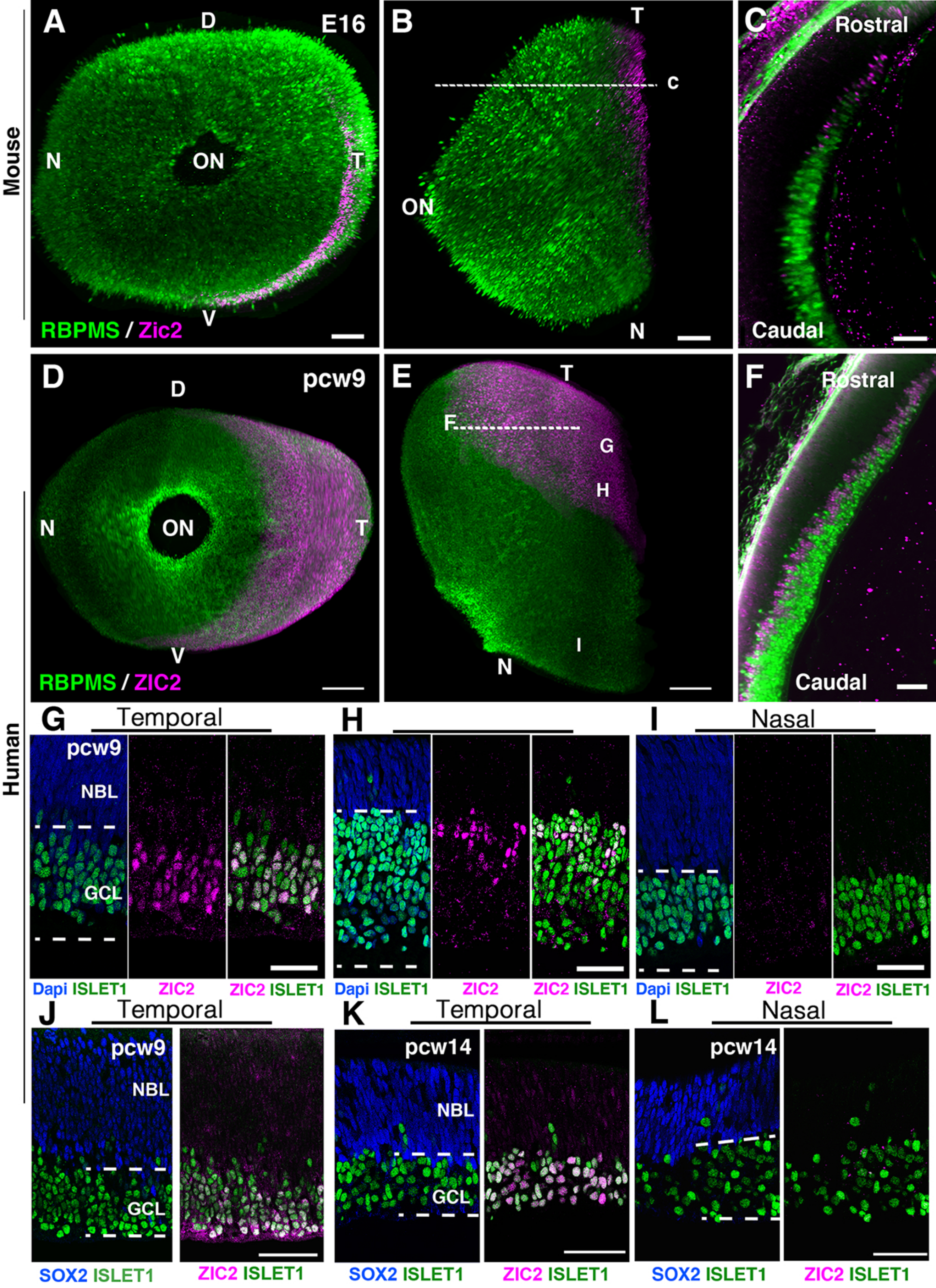
Mouse
Human
A
D
E16
N
ON
T
V
RBPMS / Zic2
B
T
c
ON
N
C
Rostral
Caudal
D
D
pcw9
N
ON
T
V
RBPMS / ZIC2
E
T
F
G
H
I
N
F
Rostral
Caudal
G
Temporal
pcw9
NBL
GCL
Dapi ISLET1
ZIC2
ZIC2 ISLET1
H
Dapi ISLET1
ZIC2
ZIC2 ISLET1
I
Nasal
Dapi ISLET1
ZIC2
ZIC2 ISLET1
J
Temporal
pcw9
NBL
GCL
SOX2 ISLET1
ZIC2 ISLET1
K
Temporal
pcw14
NBL
GCL
SOX2 ISLET1
ZIC2 ISLET1
L
Nasal
pcw14
SOX2 ISLET1
ZIC2 ISLET1

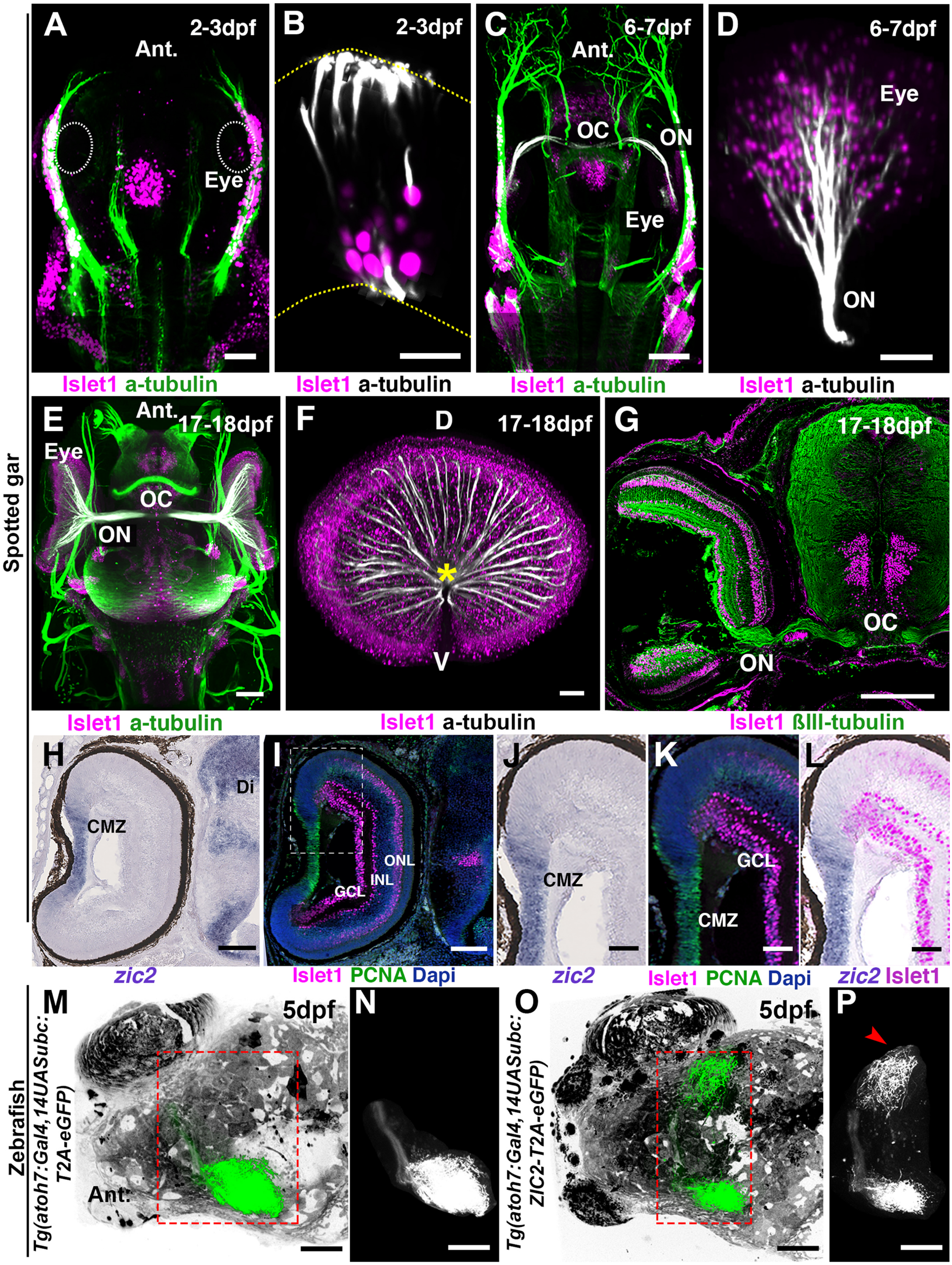

A
2-3dpf
Ant.
Eye
B
2-3dpf
C
6-7dpf
Ant.
OC
ON
Eye
D
6-7dpf
Eye
ON
Islet1 a-tubulin
Islet1 a-tubulin
Islet1 a-tubulin
Islet1 a-tubulin
E
Ant.
17-18dpf
Eye
OC
ON
F
D
17-18dpf
V
G
17-18dpf
OC
ON
Spotted gar
Islet1 a-tubulin
Islet1 a-tubulin
Islet1 ßIII-tubulin
H
Di
CMZ
I
ONL
INL
GCL
J
CMZ
K
GCL
CMZ
L
zic2
Islet1 PCNA Dapi
zic2
Islet1 PCNA Dapi
zic2 Islet1
M
5dpf
Ant.
N
O
5dpf
P
Zebrafish
Tg(atoh7:Gal4,14UASubc:T2A-eGFP)
Tg(atoh7:Gal4,14UASubc:ZIC2-T2A-eGFP)

Table S1. Comprehensive table summarizing the antibodies and probes sequences.

In situ probes						
Name	**Sequence**			**RRID**	**Dilution**	**In situ hybridization**
L-zic1 fwd	ACCTCCAGACATCACTCAAC			n/a	1:200	Cryosections
L-zic1 rev	GGAACACTCTTCCCAGAAAC			n/a	1:200	Cryosections
L-zic2 fwd	AAACTTAACCACGACCTCTCTC			n/a	1:200	Cryosections
L-zic2 rev	CTCGTGCATTGTGCTGAAAG			n/a	1:200	Cryosections
L-zic5 fwd	CTTTGAGCAAGAGGAATCCGGC			n/a	1:200	Cryosections
L-zic5 rev	CCTGCCGCGATGTTCACATTTA			n/a	1:200	Cryosections
L-efnb2 fwd	TCCCCATTATGAGAAGGTGAGCGG			n/a	1:200	Cryosections
L-efnb2 rev	ACAGGCTACCACTTCAGAAGGCAG			n/a	1:200	Cryosections
L-ephb1 fwd	AGAACCTGAACACAATCCGCAC			n/a	1:200	Cryosections
L-ephb1 rev	ACAGTTTAATGGGCACGTCCAC			n/a	1:200	Cryosections
zf-zic2a fwd	ACAACAATCTGTCGCCTTCCTC			n/a	1:200	whole-mount
zf-zic2a rev	ACAAATGCCCCTGTTTAGCCC			n/a	1:200	whole-mount
zf-zic2b fwd	TCTTCCGCTACATGCGACAAC			n/a	1:200	whole-mount
zf-zic2b rev	GCAACACCGACATGCTGAGAAC			n/a	1:200	whole-mount
zf-ephb1 fwd	CGCGTGTGGATGGATTACGG			n/a	1:200	whole-mount
zf-ephb1 rev	CATCCCCACCAGCTGGATCA			n/a	1:200	whole-mount
zf-atoh7 fwd	GGAGAAGTTTGAGAGTGCTATGCGG			n/a	1:200	whole-mount
zf-atoh7 rev	CGACTTTGAGCTGAGCACACACC			n/a	1:200	whole-mount
zf-rx2 fwd	GATACCATGAACATGGTGGACGATGG			n/a	1:200	whole-mount
zf-rx2 fwd	CCATCGACTGAATGTGCTCCTTGG			n/a	1:200	whole-mount
Primary antibodies						
Antigen	**Species**	**Catalog #**	**Company**	**RRID**	**Dilution**	**Immunohistochemistry**
Islet1	Rabbit	GTX128201	GeneTex	Ab_2868422	1:300	Cryosections/whole-mount
Acetylated-tubulin	Mouse	T6793	Sigma	Ab_477585	1:300	Cryosections/whole-mount
PCNA	Mouse	P8825	Sigma	Ab_477413	1:500	Cryosections
Islet1+2	Mouse	39.4D5	DSHB	Ab_2314683	1:50	Cryosections
GFP	Chicken	GTX13970	GeneTex	Ab_371416	1:5000	whole-mount
Rbpms	Guinea Pig	ABN1376	Millipore	Ab_2687403	1:400	Cryosections/flat-mount/ whole-
Zic2	Rabbit	Ab150404	Abcam	Ab_2868423	1:300	Cryosections/flat-mount/ whole-
Sox2	Goat	Sc17320	Santa-Cruz	Ab_2286684	1:300	flat-mount
EphB1	Mouse	MAb EfB1-3	DSBH	Ab_2314357	1:5	Cryosection
Secondary antibodies						
Anti-Rabbit cy3	Donkey	711-165-152	Jackson ImmunoResearch	Ab_2307443	1:500	cryosections/whole-mount
Anti-Rabbit Alexa Fluor 647	Donkey	711-605-152	Jackson ImmunoResearch	Ab_2492288	1:500	cryosections/Flat-mount/whole-mount
Anti-Goat Alexa Fluor 488	Donkey	A11055	Life Technologies	Ab_2534102	1:500	cryosections/Flat-mount/whole-mount
Anti-Goat Alexa Fluor 555	Donkey	A21432	Life Technologies	Ab_2535853	1:500	cryosections/Flat-mount/whole-mount
Anti-Goat Alexa Fluor 647	Bovine	805-605-180	Jackson ImmunoResearch	AB_2340885	1:600	cryosections
Anti-Goat cy3	Donkey	705-165-147	Jackson ImmunoResearch	Ab_2307351	1:500	cryosections/Flat-mount/whole-mount
Anti-mouse Alexa Fluor 488	Donkey	A21202	Life Technologies	Ab_141607	1:500	cryosections/Flat-mount/whole-mount
Anti-Guinea-Pig Alexa cy3	Donkey	706-165-148	Jackson ImmunoResearch	Ab_2340460	1:500	cryosections/Flat-mount/whole-mount
Anti-mouse Alexa Fluor 647	Donkey	715-605-150	Jackson ImmunoResearch	Ab_2340862	1:500	cryosections/Flat-mount/whole-mount
Anti-Mouse, Alexa Fluor 635	Goat	A31574	Life Technologies	Ab_2536184	1:500	cryosections
Anti-Rabbit, Alexa Fluor 568	Goat	A11036	Life Technologies	Ab_10563566	1:500	cryosections
Anti-Mouse, Alexa Fluor 568	Goat	A11004	Life Technologies	Ab_2534072	1:500	cryosections
Alexa Fluor 488 anti-chicken	Goat	A11039	Life Technologies	Ab_142924	1:500	cryosections
Tracers						
Cholera toxin subunit B-AlexaFluor555	n/a	C22843	Life technologies	n/a	2 μg/μl	Whole-mount
Cholera toxin subunit B-AlexaFluor647	n/a	C34778	Life technologies	n/a	2 μg/μl	Whole-mount